2016

Characterizing the El Nino Southern Oscillation (ENSO) variability using Sr/Ca-based SST and δ18O-derived SSS from the Southwest Pacific

Grace Duke

Mentors: Dr. Michael Evans*, Dr. Andrew Lorrey+

April 25, 2016

GEOL394H

Table of Contents

Contents: Tables and Figures

1. **ABSTRACT:** The scarcity of oceanic observations limits the scientific understanding of ENSO's natural variability. ENSO is a source of prominent interannual variability and it is unknown how its behavior may change with increasing global temperatures (Stocker et al., 2013). This research studied the interannual variability in reconstructed SST and SSS anomalies based on detrended Sr/Ca and $\delta^{18}O$ anomalies inputted into equation from Ren et al. (2002). New data from Aitutaki was examined along with pre-existing data from Rarotonga, Fiji, and New Caledonia. The Aitutaki data was found to be statistically different from the other sites, with p-values below the 0.05 significance level. The interannual frequency and period of New Caledonia, Fiji, and Rarotonga was chosen to be investigated in depth because those sites significantly correlated with SOI, an index used to ENSO phase events. Over a moving centered 30-year period, the measurements calculated were the number occurrences in which a data series fell above or below zero and the average period of those occurrences. The analysis found that the natural interannual frequency of the SPCZ, which is significantly correlated to ENSO, has not varied significantly over time, ranging between 4-9 occurrences of below/above zero periods in a 30-year period. The average Sr/Ca, $\delta^{18}O$, Sr/Ca-SST, and $\delta^{18}O$-SSS had not changed significantly between the late 19th century and the late 20th century. Based on the interannual analysis, there is evidence that suggests the SPCZ has expanded eastward, agreeing with previous studies (Linsley et al, 2006; Wu et al., 2013). Based on the frequency of times that fell above or below zero, the analysis determined the potential for either ENSO phase has become more equal over time. Although this study examined the natural frequency of ENSO, further research is needed to investigate the inter-site relationships in SSS anomalies across the southwest Pacific to better understand variations in ENSO's intensity.

2. Introduction

The El Niño Southern Oscillation (ENSO) is a prominent source of interannual climate variability that arises from changes in the strength of the atmospheric-oceanic circulation in the equatorial Pacific. The warm and cold phases of ENSO, commonly referred to as El Niño and La Niña, impact global precipitations and temperatures patterns via teleconnections (Vincent, 1993; Widlansky et al., 2010). With rising surface temperatures, there will likely be an intensification in rainfall associated with ENSO (Stocker et al., 2013; Wu et al., 2013) and a eastward shift in certain teleconnection patterns (Stocker et al., 2013). However, these projections presented by the Intergovernmental Panel on Climate Change (IPCC) have medium to low confidence because there is considerable debate about how warming temperatures will impact the intensity and frequency of ENSO (Stocker et al., 2013).

The underlying natural mechanisms and forcings that cause climate variability are important for the better prediction and mitigation of climate change, but it can be difficult to achieve due to a lack of observations. Although oceans cover the majority of the Earth, oceanic instrumental observations made prior to the late 20th century are scarce (Figure 1; Delcroix et al., 2011). Figure 1a displays the distribution of accumulated sea surface salinity (SSS) data records (e.g. ships, in-situ data, moorings, Argo floats) collected in the tropical Pacific from 1950-2008 based on a 5-day bin, 1°x1° grid (Delcroix et al., 2011). From 1950 to 1969, very few SSS measurements were collected for the majority of the tropical Pacific (figure 1a). Locations with multiple observations include prominent shipping lanes or near land masses (Figure 1). The scarcity of direct observations complicates the understanding of climate variability. Several methods are used to extend the spatial and temporal coverage of information: model simulations, data assimilation, data compilations, and data reconstructions.

The advantage of model simulations is their discrete temporal and spatial resolution, allowing large-scale patterns to be tracked and better observed. Models are limited by their parameters, boundary conditions, and programmed formulas; therefore, to test the scientific understanding used to construct models, the output of models must be compared to observations. Models simulate climate variables by

employing knowledge of environmental forcings and physical properties to climate processes. The IPCC relies on various simulations to assess climate change and formulate a report on the state of the climate (Stocker et al., 2013). The IPCC's Fifth Assessment Report states there is an overall high confidence in the ability of models to reproduce the magnitude and patterns of sea surface temperature (SST), but are less capable representing precipitation patterns (Stocker et al., 2013). They found that most models

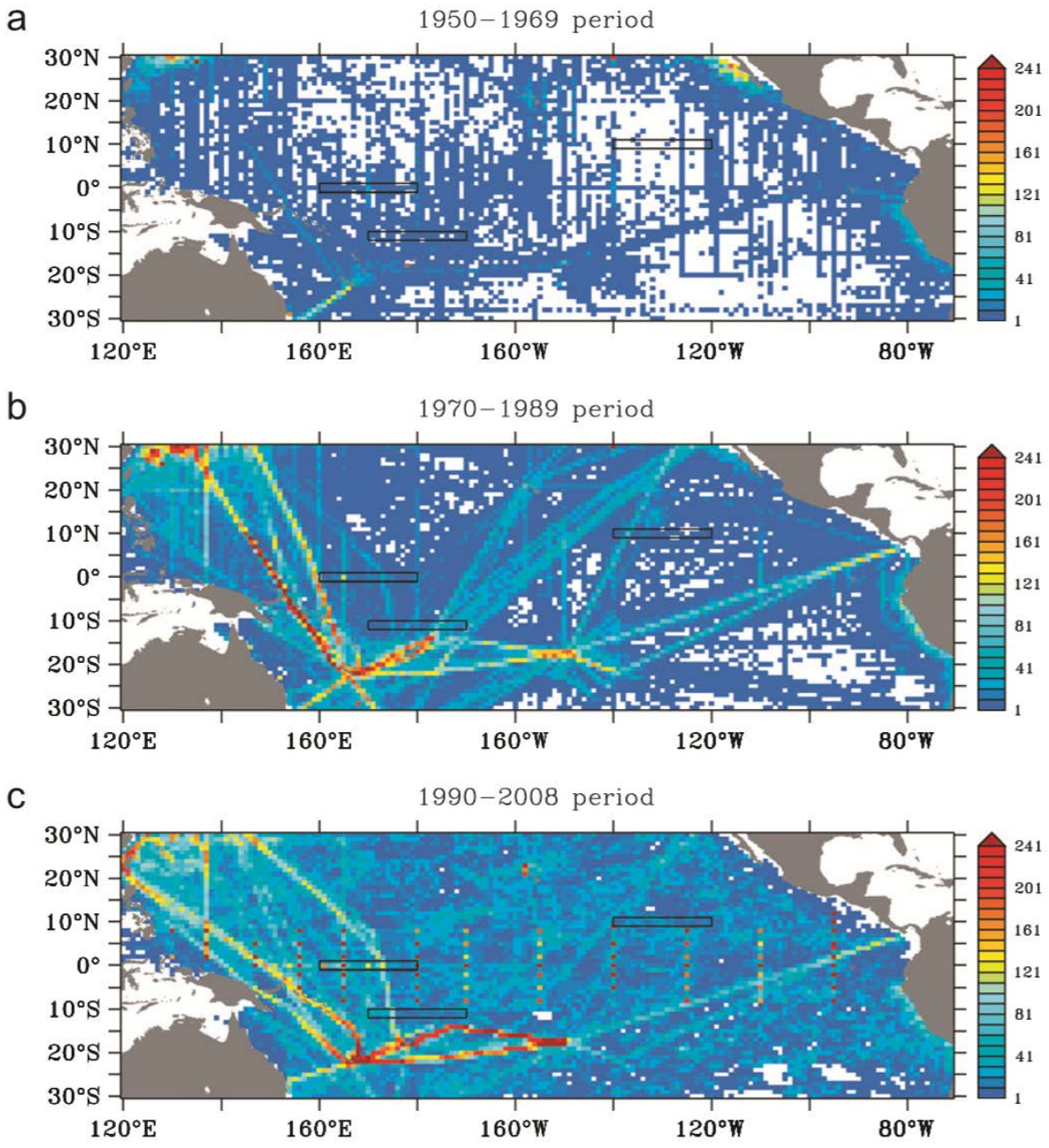

Figure 1: Spatial distribution of the number N of 5-day bins with SSS observations per 1° x 1° grid box for (a) 1950–1969, (b) 1970–1989, and (c) 1990–2008 time periods, respectively. The color codes on the color bar are the N stretch from dark blue (N¼1) to dark red (NZ241). *Figure from Delcroix et al., (2011).*

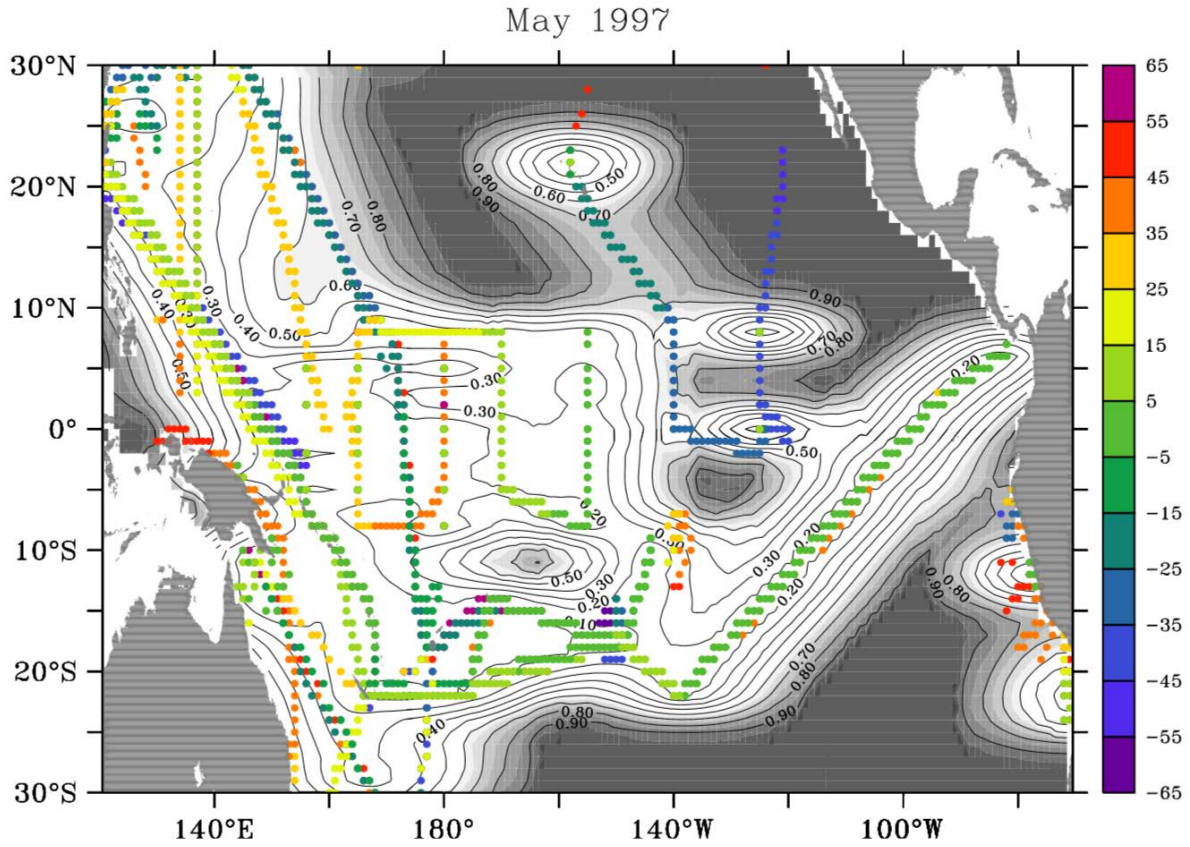

Figure 2: Spatial distribution of the SSS normalized errors in May 1997. Contour intervals are 0.1, and shaded grey areas show error values greater than 0.6. The small colored circles represent all the 5-day bins SSS values that were used to compute the errors, with their color code denoting the distance in days from May 15, 1997. *Figure from Delcroix et al., (2011).*

underestimate the response of anomalous precipitation to temperature variability, especially in the tropics (Stocker et al., 2013). Causes of model error include internal model variability and uncertainty in scientific understanding (Delcroix et al., 2011; Stocker et al., 2013).

Data assimilations use observations to correct a model's output, serving as an initial guess to the environmental condition of the ocean for further analysis (Carton and Giese, 2008). Carton and Giese (2008) describe the process used to produce the Simple Ocean Data Assimilation (SODA). They began SODA's analysis with a "state forecast" from an ocean general circulation model. Then, they introduced incremental corrections based on the difference between the forecast and observations during a 10-day assimilation cycle running from 1958-2001 (Carton and Giese, 2008). This process reduces model bias, but the reanalysis results experience errors related to changes in how observations are measured and the availability of observations (Carton and Giese, 2008).

Delcroix et al. (2011) complied a 1° x 1° gridded SSS data set for the tropical Pacific from instrumental records ranging from 1950-2008. They noted that error increases in areas with less observations. To determine the reliability of a gridded SSS variance value, they calculated the normalized error at each grid point (Delcroix et al., 2011). Delcroix et al. (2011) mapped the normalized errors and the 5-day bins used to calculate normalized errors for May 1997 (figure 2). The shaded gray areas that distinguish errors greater than .6 in figure 2 have very few 5-day bins, illustrating that fewer observations increase the computed error. In general, the availability of observations and the uncertainty in scientific understanding are sources of error and restrict the confidence scientists can assign to analyses and results.

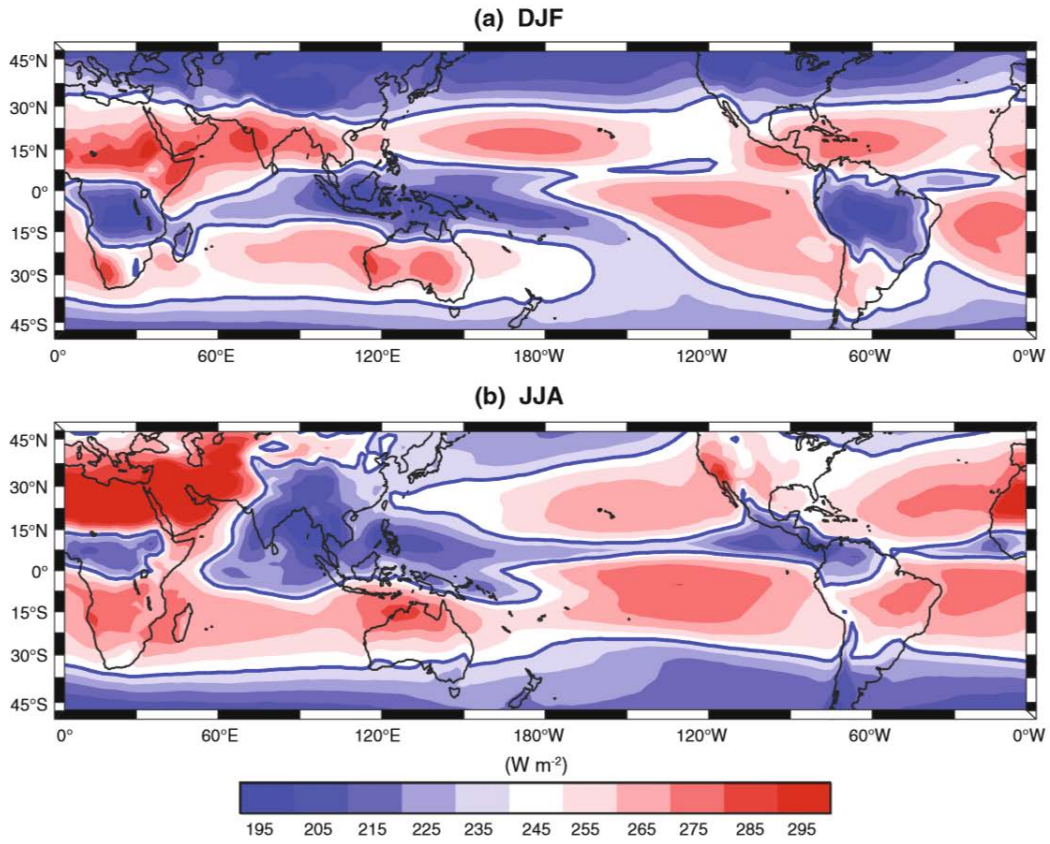

Figure 3: Global climatology (1982–2008) of OLR (W m-2) for a DJF and b JJA. 240 W m-2 OLR anel contour outlined by blue lines in each panel. *Figure from Widlansky et al. (2010).*

Geochemical variations within natural archives (e.g. ice cores, tree rings, sediment layers, coral) are measured and correlated to climate variables to produce data reconstructions. These data sets add robustness to the spatial and temporal coverage of existing climate records, providing further observational information on past climate change to make future projections. For instance, the strontium to calcium ratio (Sr/Ca) and the oxygen isotopic composition ($\delta^{18}O$) within a coral's aragonite ($CaCO_3$) skeleton are used to reconstruct SSS and SST anomalies (Weber, 1973; Smith et al., 1979; Gagan et al., 1998; Ren et al., 2002; Linsley et al., 2006; Gorman et al., 2012; Wu et al., 2013). Sr/Ca measurements are negatively correlated to SST and $\delta^{18}O$ depends primarily on SST and the $\delta^{18}O$ of seawater, which is positively proportional to SSS. The variability of $\delta^{18}O$ deconvolves into components associated with the effect of SST and SSS. The SST component can be removed using a reconstructed SST anomalies derived from Sr/Ca anomalies, leaving a residual signal associated with SSS variability (Gagan et al., 1998; Ren et al., 2002; Gorman et al., 2012).

The $\delta^{18}O$-SSS and Sr/Ca-SST reconstructions add to the growing network of climate proxy reconstructions, which all contribute to expanding the coverage of observations and improving the scientific understanding of the climate's natural variability. ENSO variability can be related to the variability of $\delta^{18}O$-SSS anomalies based how ENSO phases impact a regional climate feature called the South Pacific Convergence Zone (SPCZ), which influences SSS values in the region (Linsley et al., 2006). The SPCZ, an area of near-surface convergence that extends from the western equatorial Pacific and southeasterly as 30°S, 120°W (Vincent et al., 1993), is characterized by a persistent cloud band and high levels of rainfall;

its position is identifiable by low outgoing radiation (Figure 3). By tracking changes in SSS over a given period, the interannual variability of a SSS signal can be correlated to ENSO and the SPCZ shifting position.

In this study, the variability of the Sr/Ca and $\delta^{18}O$ anomalies within a coral's aragonite ($CaCO_3$) skeleton was examined to deduce whether the frequency and intensity of ENSO increased during the last two centuries in the southwest tropical Pacific. New data presented in this paper were taken from the stony *Porites* core, ATC13019B, collected from the eastern shore of Aitutaki (18.85°S, 159.79°W), an island of the southern Cook Islands in the Southwest Pacific. The null hypotheses are:

1. Climatological averages and anomalies of SSS and SST from the Southwest Pacific have no statistical difference between the late 19th century and the 20th century.
2. There is no significant difference in the frequency of ENSO warm phases and cold phases between late 19th century and the late 20th century.

The remaining paper is as follows: section 3 is background on the regional climate and climate proxies; section 4 describes the data I used, including the new ATC13019B data and pre-existing measurements; section 5 outlines the methodology used for to produce coral-based simulated climate proxies; section 6 and 7 presents results and discussion; and section 8 is a conclusion.

3. Background

3.1 Regional Climate

The tropical Pacific is characterized by a zonal sea surface temperature (SST) gradient and areas of low-level atmospheric convergence along the equator, the Inter-Tropical Convergence Zone (ITCZ), and in the southwest, the South Pacific Convergence Zone (SPCZ). Strong trade winds transport warm equatorial waters into a region known as the Western Pacific Warm Pool, where the amassed water averages 28 °C or higher (Vincent, 1998; Quinn et al., 2006) and the convergence of warm, moist air fuels strong convection producing large amounts of precipitation and latent heat export. In the eastern equatorial Pacific, SST are cooler (24-20 °C) due to cold, deep ocean waters upwelling along the coast of South America and circulating equatorward with waters from higher latitudes. The position of SPCZ in the far western Pacific aligns zonally with the SST gradient, inducing a pressure gradient and convergence (Kiladis et al., 1989; Vincent, 1993; Widlansky et al., 2010). As the SPCZ extends southeasterly into the subtropics, its diagonal position is dependent on mid-latitude circulation (Kiladis et al., 1989; Vincent, 1993; Widlansky et al., 2010).

The warm and cold phases of ENSO are identifiable by distinctive patterns of SST anomalies in the equatorial Pacific. During the warm phase, atmospheric-oceanic circulation in the equatorial Pacific weakens, causing the trade winds and oceanic upwelling to slacken and warmer surface waters to extend into the eastern Pacific. The high rainfall, typical to the western Pacific, moves into the central Pacific as temperatures cool in the west but warm in the east. In contrast, the atmospheric-oceanic circulation strengthens during the cold phase of ENSO, warming SST further in the west and causing above average precipitation in the far western Pacific.

Depending on the phase of ENSO, the SPCZ will shift its position, causing anomalously high (low) SSS in areas accustom (unaccustomed) to the SPCZ's high rainfall. When circulation weakens during the warm phase, the SPCZ migrates northeasterly, its diagonal portion becoming more zonal and inducing anomalously high SSS in the region it normally resides. However, the stronger winds during the cold phase cause the SPCZ to move southwesterly, resulting in below average SSS for the Southwest Pacific.

3.2 Porites Corals

The isotopic and elemental variations measured within the aragonite skeleton of the reef-forming order, Scleractinia, are commonly correlated to oceanic variables, such as SST and SSS, to produce climate reconstructions. The massive, surface-dwelling coral genus, *Porites*, is often used for paleoclimate reconstructions because they commonly grow to a large size, old age, and in a range of temperature conditions across the Indo-Pacific (Pichon, 2011). Growth factors include temperatures ranging from 15-32 °C, exposure to sunlight, and salinity. Most *Scleractinian* corals, including *Porites*, have a symbiotic

relationship with photosynthesizing micro-organisms, zooxanthellae, that live within their cell walls and provide the nutrients and energy required for growth (Done et al., 2011). The availability of sunlight controls how well the zooanthellae photosynthesizes, and therefore, the turbidity of water, latitude, and water depth determine the location and the rate at which a coral may grow.

The annual growth of a coral is identified by a sequential pair of density bands, one lightly-colored followed by a darker, and denser band. The change in density represents a change in the growth rate of coral; the lighter, less dense band corresponds to the rapid growth period of the year whereas the darker band corresponds to slower growth rates (Lough and Barnes, 2000). These bands, some of which are highlighted in red in figure 4, may be counted to determine the age of a coral.

3.3 Climate Proxies

The negative correlation between SST and the ratio between strontium and calcium (Sr/Ca) within the coral aragonite ($CaCO_3$) skeleton is well established (Weber, 1973; Smith et al., 1979; de Villiers et al., 1994; Lough and Barnes, 2000; Linsley et al., 2004, 2006; Corrège, 2006; Quinn et al., 2006; Delong et al., 2012). Strontium (Sr^{2+}) is incorporated into the coral's skeleton by substituting in for calcium (Ca^{2+}) as aragonite precipitates from the extracellular calcification fluid that lies between the skeleton and the thin cell layer that lies above (Cohen et al., 2001; Allison et al., 2001; Allison et al., 2013). Strontium's incorporation into aragonite is impacted by SST, with low (high) temperatures leading to higher (lower) strontium concentrations because cooler temperatures drive the $SrCO_3$ reaction towards the formation of $SrCO_3$, the more stable product at lower temperatures (Ruiz-Hernandex et al., 2010).

In conjunction with SST anomalies reconstructed from Sr/Ca, the influence of SSS on the oxygen isotopic composition ($\delta^{18}O_{coral}$) of an aragonite skeleton can be isolated and used to track changes in local rainfall activity. SSS represents the amount of dissolved salt content within the upper few decameters of

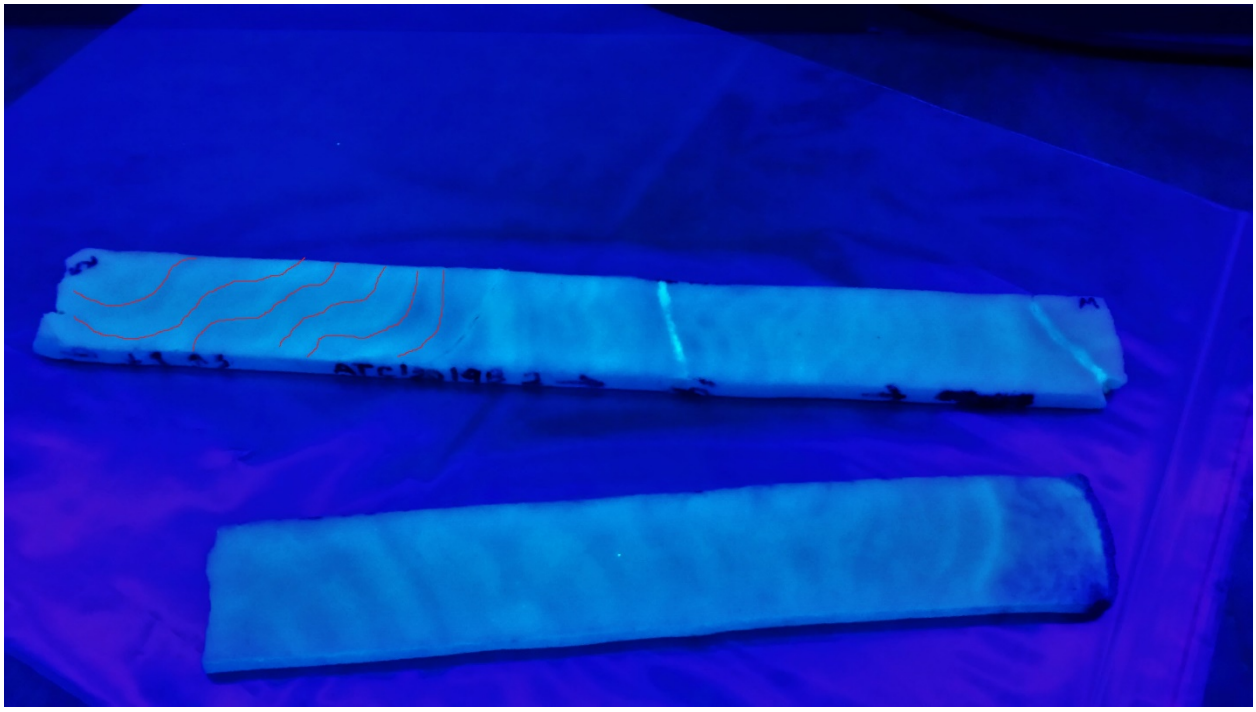

Figure 4: Enhanced image of coral sample, ATC13019B, placed under Ultra-Violet light (photo by Grace Duke). Red lines highlight several alternating density bands in the upper coral slab.

the ocean, where the water is well-mixed and generally uniform (Delcroix et al., 2011). Among the three stable oxygen isotopes, the ratio between the heaviest isotope, ^{18}O, and the lightest, ^{16}O, in seawater is positively correlated to SSS because the equilibrium vapor pressure of water bonded with ^{18}O ($H_2{}^{18}O$) is

slightly lower than the vapor pressure of water bonded with ^{16}O (Fairbanks et al., 1997). As a result, evaporated water molecules are slightly depleted in $H_2{}^{18}O$ in relation to the seawater. The SST component of $\delta^{18}O_{coral}$ derives from the temperature-dependence of oxygen isotope fractionation during carbonate precipitation from seawater, with less fractionation at higher temperatures (Weber and Woodhead, 1972).

Whether the extension rate (mm $year^{-1}$) or calcification rate (g cm^{-2} $year^{-1}$) of coral contribute significantly to the variability of paleoclimate reconstructions is highly debated (Weber, 1973; Smith et al., 1979; de Villiers et al., 1994; Lough and Barnes, 2000; Cohen et al., 2001; Corrège, 2006). Another source of error currently being investigated is the effect of "bio-smoothing," the attenuation of isotopic and elemental signals due to aragonite precipitation in the tissue layer (Gagan et al., 2012). The dampening of the geochemical signal results in the magnitude of climatic trends being overestimated (Gagan et al., 2012). Quinn et al. (2006) examined the Sr/Ca and $\delta^{18}O$ measurements from Rabual, Papua New Guinea, which lies in the Western Pacific Warm Pool. They noted the calculated trend in Sr/Ca-based SST, which is equivalent to a ~.7°C cooling, from 1867-1997 is improbable considering other warming trends noted in the area (Quinn et al., 2006).

Diagenesis is the recrystallization of the aragonite skeleton after deposition by either secondary calcite or aragonite (McGregor and Gagan, 2003; Allison et al., 2007). Secondary aragonite growth gives the impression of cool climatic conditions and is a characteristic of early marine diagenesis (McGregor and Gagan, 2003; Allison et al., 2007; McGregor and Abram, 2008; Nothdruft and Webb, 2009). Whereas, secondary calcite results in seemingly warm climatic conditions and is found in young and fossil corals alike (McGregor and Abram, 2008). To test whether a coral core is pristine, diagenetic tests such as X-ray Diffractometry and Cathodoluminescence Microscopy serve as an initial test to detect micro amounts of calcite growth (McGregor and Gagan, 2003; McGregor and Abram, 2008; Frankowiak et al., 2013). In order to detect secondary aragonite, the textural variations and crystallographic patterns in the coralline skeleton must be examined using methods such as scanning electron microscopy (SEM) and petrographic analysis. Diagenetic tests are essential because even small level of diagenesis can significantly influence paleoclimate reconstructions (McrGregor and Gagan, 2003).

4. Methods

4.1 Data

ATC13019B, a 53 cm-long core, was collected from a microatoll on the eastern shore of Aitutaki by University of Maryland Ph.D. candidate Alex Lopatka and associate professor Dr. Michael Evans with fellow collaborators: Dr. Andrew Lorrey*, Dr. Helen McGregor**, and Dr. Melinda Allen^{+}. The coral was sectioned and processed by Lopatka at the National Institute of Water and Atmospheric Research in Auckland, New Zealand. One section of ATC13019B was milled at 1 mm intervals along the axis of maximum growth, producing approximately 1000 ug aliquots for each interval for geochemical analyses. Diagenetic testing revealed a skeletal composition of 100% aragonite and Th/U dating determined a minimum growth year of 1877 ± 2 CE. With assistance from Dr. Lorrey and the Th/U date as reference, the age of ATC13019B was dated from the start of 1885 CE to the middle of 1920 CE. As a reference point, a large negative anomaly in the Sr/Ca data series was correlated to a strong ENSO cold phase during the winter of 1917-1918.

The oxygen isotopic composition ($\delta^{18}O$) was measured using an Isoprime continuous flow Isotopic Ratio Mass Spectrometer (Isoprime House, UK) at the University of Maryland with validated precision of approximately 0.1‰ (Evans et al 2016, revised). The $\delta^{18}O$ is defined as:

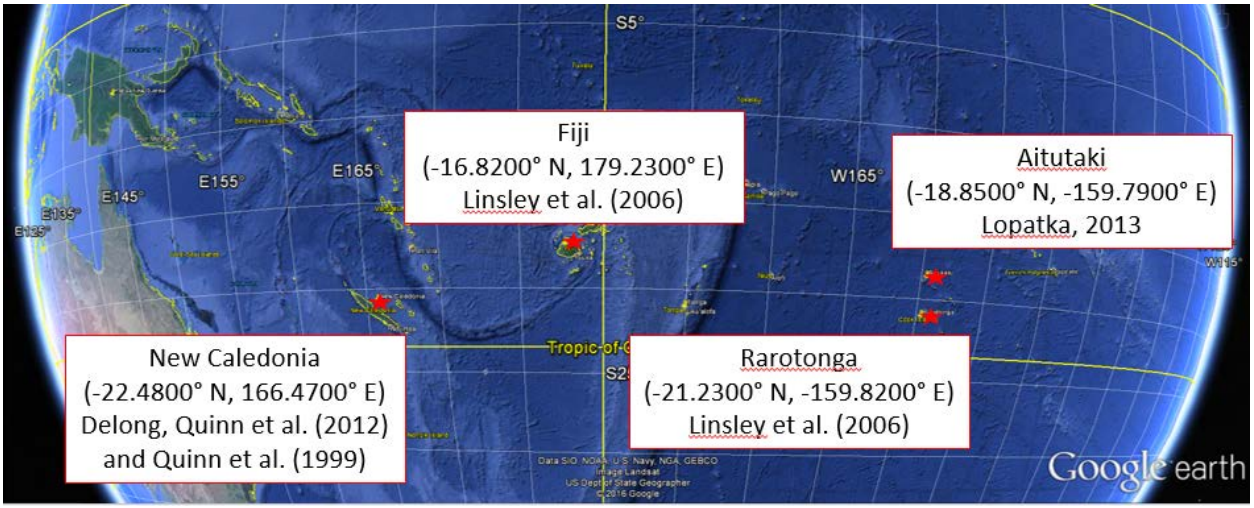

Figure 5: Map of the South Pacific shows the geolographical positions of sites studied.

$$\delta^{18}O = \left(\frac{(\frac{^{18}O}{^{16}O})_{sample}}{(\frac{^{18}O}{^{16}O})_{standard}} - 1 \right) * 1000\%$$

The isotopic composition of a sample in a set of 12, each weighed to 100 ug, were analyzed with two in-house standards ($\delta^{18}O$ values of 8.71 and 21.73 ‰), which are referenced to the international standard Vienna Peedee Belemnite. The Sr/Ca samples, weighed to 500 ug, are dissolved in 3-5 mL of 2% nitric acid in order to be analyzed at the Australian National University on a Varian Vista Pro Axial Inductively Coupled Plasma Atomic Emission Spectrometer (ICP-AES).

In addition to Aitutaki data, pre-existing Sr/Ca and $\delta^{18}O$ data series from three sites were used to study hydrological variability across the Southwest Pacific. Data series were selected from the National Climate Data Center's database of paleoclimate data series based on their location in the SPCZ region, age, and data quality. Their age needed to span the 19th century and into the 20th century in order to make comparisons between the two centuries. Sites included New Caledonia, Fiji, and Rarotonga (Figure 5).

The New Caledonia data presented here originates from two different pre-existing studies. Delong et al. (2012) composited monthly Sr/Ca data (1653:1994) from five *Porites* cores collected from the shallow waters off the shore of Amédée Island, New Caledonia (-22.48° N, 166.47° E). Measurements were assigned an uncertainty of ±0.018 mmol/mol, combining the analytical precision of the instrument used to measure Sr/Ca and precision of the sampling process (Delong et al., 2012). Quinn et al. (1999) performed a $\delta^{18}O$ analysis (1662-1987) on a *Porites* core collected from Amédée Island and determined the uncertainty associated with the seasonally sampled measurements to be 0.1 per mil. The Fiji data (1785-1987), analyzed at an annual resolution with a relative standard deviation of .2%, was originally used by Linsley et al. (2006) after two cores were collected from Savusavu Bay, Vanua Levu, Fiji (-16.82° N, 179.23° E). The Rarotonga data (1730:1987) were also used by Linsley et al. (2006) based on *Porites* cores from Rarotonga (-21.23° N, -159.82° E) with a relative standard deviation of .15%.

4.2 Data Processing

As an initial step, annually averaged $\delta^{18}O$ and Sr/Ca values were computed for each site and seasonal averages for those sites with monthly or seasonal resolution. After the annual average was calculated for each data series, the pre-existing data series were detrended by first removing the long-term

trend, and then removing the decadal trend. Detrending isolates the interannual variability influenced by ENSO (appendix: table 1 and table 2). Because the Aitutaki record is 36 years long, only linear detrending was performed. In order to make comparisons between Southwest Pacific sites, data series were standardized over time periods of interest using the corresponding mean and standard deviation.

Assuming that Sr/Ca is solely dependent on SST, Sr/Ca-based SST anomalies were reconstructed using the following equation:

$$\Delta SST = \frac{\Delta \frac{Sr}{Ca}}{\left(d\frac{\frac{Sr}{Ca}}{dSST} \right)} \qquad equation\ 1$$

where ΔSr/Ca and ΔSST are the anomalies, deviations from the climatological mean, and (∂Sr/Ca)/∂SST is the rate of change in Sr/Ca with respect to SST (Ren et al., 2002). Ren et al. (2002) derived a SSS anomaly reconstruction for Rarotonga, about 270 Km south-southeast of Aitutaki, based on Sr/Ca and $\delta^{18}O$ measurements from several Porites corals. Ren et al. (2002) used a (∂Sr/Ca)/∂SST of -0.062 ± .008 mmol/mol/°C, which is based on the average of Sr/Ca-SST linear regression slopes (ranging from -0.0412 to -0.0815 mmol/mol/°C) reported by published studies and is similar to other reported averages (Quinn and Samson, 2002; Corrège, 2006).

To derive SSS anomalies from $\delta^{18}O$ and Sr/Ca-SST anomalies, the following equation from Ren et al. (2002) was used under the assumption that $\delta^{18}O$ is dependent only on seawater $\delta^{18}O$ and SST, the former correlated with SSS:

$$\Delta\, \delta^{18}O = \frac{\partial\, \delta^{18}O}{\partial SST} * \Delta SST + \frac{\partial\, \delta^{18}O}{\partial SSS} * \Delta SSS \qquad equation\ 2$$

where $\Delta\delta^{18}O$ is the anomaly of $\delta^{18}O$, ΔSST is the ATC13019B Sr/Ca-SST anomalies, and $(\partial\delta^{18}O)/\partial$SST and $(\partial\delta^{18}O)/\partial$SSS are the rate of change of $\delta^{18}O$ by SST (-.21 mmol/mol/°C; Ren et al., 2002) and SSS (.45 mmol/mol/psu; Thompson et al., 2011) respectively. The −0.21 (±0.02) mmol/mol/°C is the linear regression slope between SST and $\delta^{18}O$ for the common Porites genus of corals (Thompson et al., 2011) and 0.45 (+/- 0.028) permil/psu, is based on the basin-scale $\delta^{18}O_{seawater}$ vs. SSS regression estimate for the South Pacific (Thompson et al., 2011). The relative error assigned to this method as calculated by Ren et al. (2002) is 27%.

5. Results and Discussion

5.1 Uncertainty

Uncertainty in Aitutaki Sr/Ca and $\delta^{18}O$ original measurements is caused by: the method of collecting coral cores; the process of sampling coral cores; the capabilities of instruments used to measure Sr/Ca and $\delta^{18}O$; and the techniques chosen to interpret data. Variance in the concentration of Sr/Ca and $\delta^{18}O$ in seawater is insignificant because both elements are conservative species; their concentrations are constant in relation to salinity. The variability of strontium and calcium within seawater is essentially constant, contributing ≤2°C variability between various SST reconstructions from different sites around the Tropics (de Villiers et al., 1994). The variability in the Sr/Ca of seawater is due to the biological cycling

of calcium carbonate ($CaCO_3$) and the skeletal building of protozoan acentharia of celestite ($SrSO_4$) (de Villiers et al., 1994).

To quantify the uncertainty of Aitutaki data, the error involved with the instrumentation, sampling, and aging were considered. The uncertainty due to diagenesis is neglected because diagenetic testing found

Table 1: Mean Sr/Ca (mmol/mol) with standard deviation for Southwest Pacific sites during time periods of interest

Site	1885 – 1920	1952 – 1987	1785 – 1987
New Caledonia	9.23 ± 0.023	9.19 ± 0.020	9.21 ± 0.023
Fiji	9.27 ± 0.039	9.23 ± 0.027	9.27 ± 0.037
Rarotonga	9.49 ± 0.045	9.46 ± 0.042	9.46 ± 0.048
Aitutaki	8.88 ± 0.079		

Table 2: Mean d18O (per mil) with standard deviation for Southwest Pacific sites during time periods of interest

Site	1885 – 1920	1952 – 1987	1785 – 1987
New Caledonia	-4.24 ± 0.17	-4.45 ± 0.08	-4.28 ± 0.18
Fiji	-4.92 ± 0.14	-5.13 ± 0.12	-4.92 ± 0.17
Rarotonga	-4.36 ± 0.12	-4.43 ± 0.10	-4.29 ± 0.16
Aitutaki	-4.60 ± 0.16		

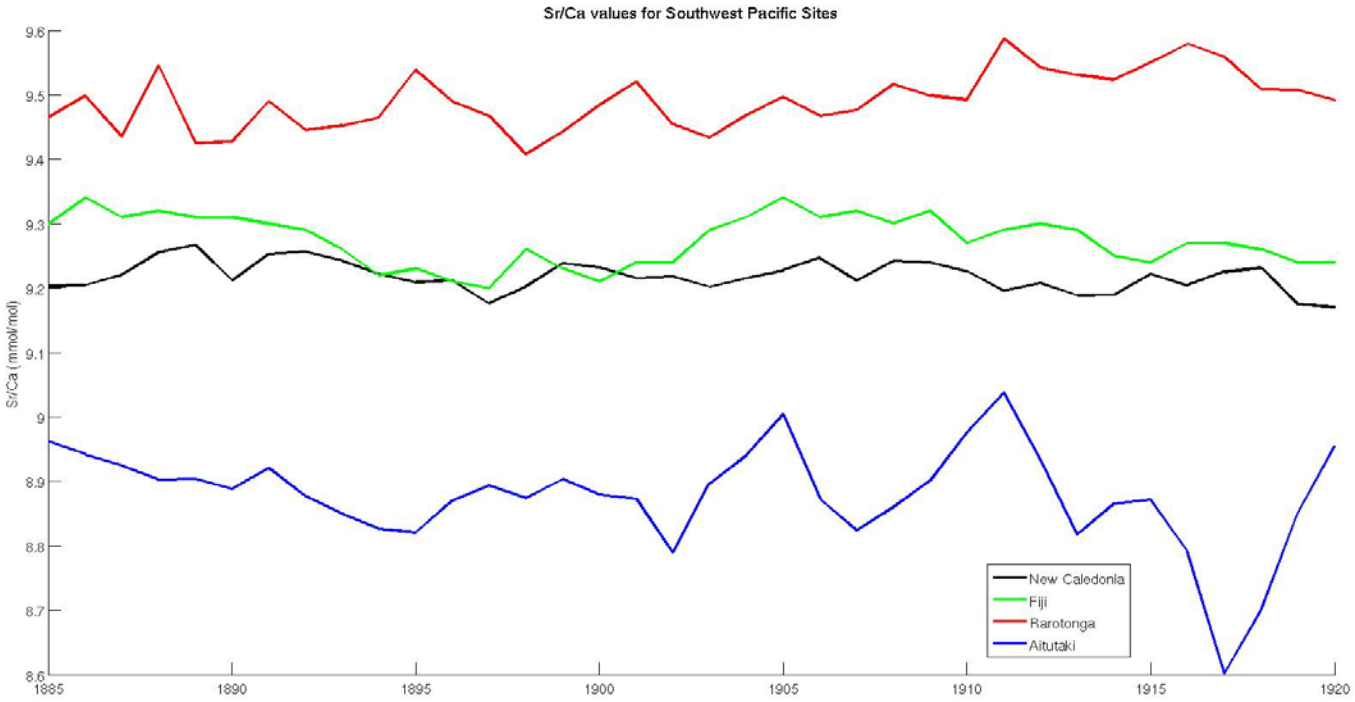

Figure 6: Original Sr/Ca-SST data for the southwest Pacific sites from 1885-1920 CE. The uncertainty associated with Rarotonga (red) is ± 1.7 mmol/mol, Fiji (green) ± 1.9 mmol/mol, New Caledonia (black) ± .018 mmol/mol, and Aitutaki ± 1.1 mmol/mol.

ATC13019B to be 100% aragonite. To quantify the sampling error, the difference between two $\delta^{18}O$ measurements corresponding to the same year was calculated for a 10-year long Aitutaki coral core, ATC13100. The average of the differences corresponds to a sampling error of 0.015%. The precision of the IRMS and ICP-AES instruments contributes .01% uncertainty to the final geochemical measurements. Additional uncertainty is acquired during the aging of the data series. To determine the sensitivity of the annual averages to which samples were assigned, the annual time series was calculated by two people and the number of samples chosen for a year varied. The resulting error was about .1%. Based on the ± 2 years associated with the TIMS date, there is a .06% uncertainty associated with the range of the Aitutaki time series. The uncertainty within the Aitutaki raw data amounts to 0.12% when all the above given uncertainties are used in the propagation of error calculation. The error with the pre-existing data and the calculations are discussed in the methods section. The error associated with the calculations is 2-3 orders of magnitude greater than the error associated with each site's data. Because of this large difference, a flat uncertainty of 27% was applied to all calculations.

5.2 Original Sr/Ca and $\delta^{18}O$ data

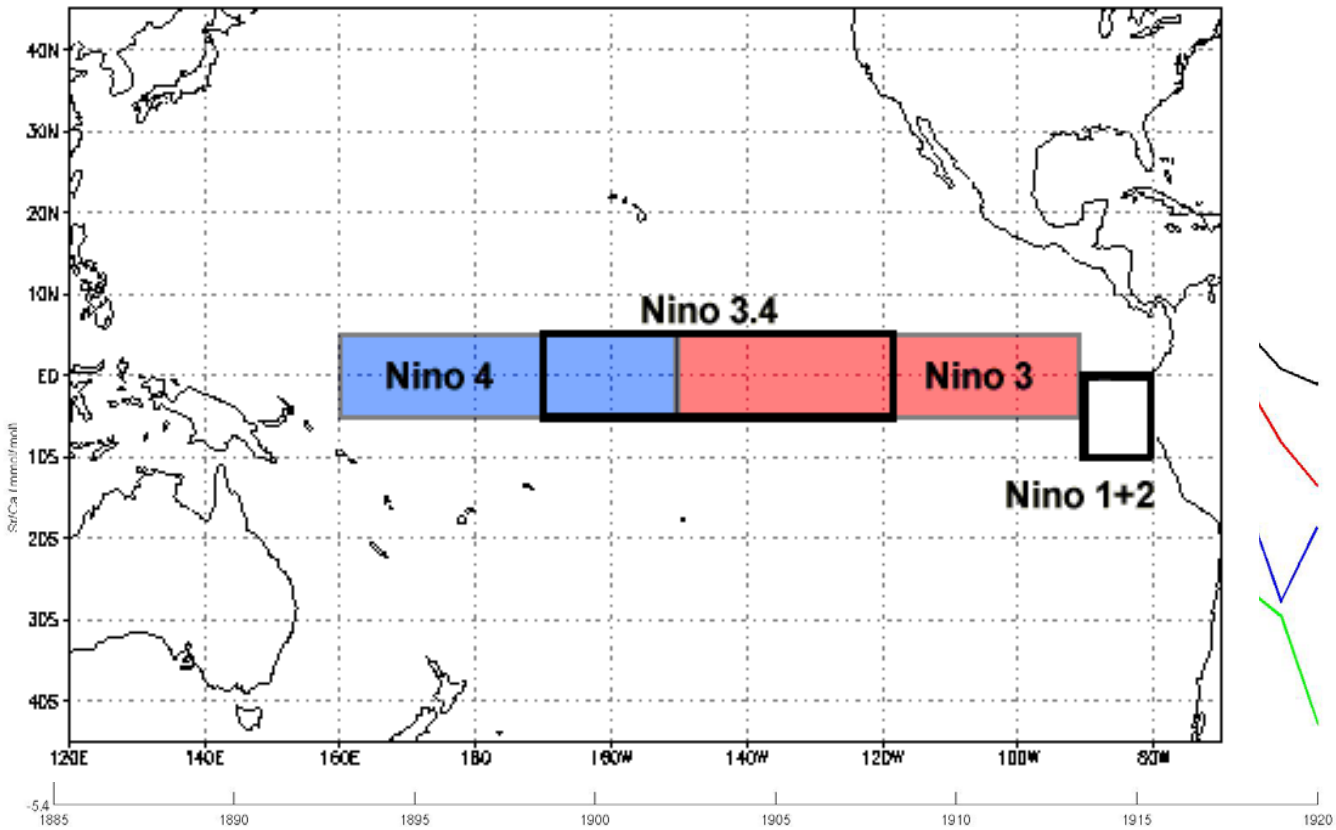

Figure 8: The Niño 3.4 Region overlaps the Niño 4 (blue) and Niño 3 region (red).

Figure 7: Original data δ^{18}O-SSS for the southwest Pacific sites from 1885-1920 CE. The uncertainty associated with Rarotonga (red) is ± 0.77 per mil, Fiji (green) ± 1.0 per mil, New Caledonia (black) ± .1 per mil, and Aitutaki ± .56 per mil.

Analysis was focused on two time periods: 1885 to 1920 based on the age of the Aitutaki data, and 1952 to 1987 based on the most current 35 year period in which all pre-existing data coincide. Figure 6 and 7 displays the original Sr/Ca and $\delta^{18}O$ values for each site for 1885-1920 CE. Each site has a distinct Sr/Ca and $\delta^{18}O$ signature, but Aitutaki Sr/Ca data display high variability from about 1905 to 1920. For each site, the change in the mean Sr/Ca from the turn of the century to the late 20th century stays within 2 sigma of each other, despite a decrease in the average between the two time periods (table 1). Similarly, the change in mean $\delta^{18}O$ is not significantly different between the two time periods, staying within two sigma of each other, although there is a slight decrease in the mean (table 2).

As mentioned before, Sr/Ca has a negative correlation with SST; consequently, a negative change in Sr/Ca corresponds to a positive rise in SST. Whereas, $\delta^{18}O$ is negatively correlated to SST and positively correlated to SSS; therefore, to interpret the trend of $\delta^{18}O$ requires the consideration of both factors. A decrease in $\delta^{18}O$ across the southwest Pacific may be associated with a rise in temperature, a freshening of the region's surface waters due to an increase in precipitation, or a mixture of both. The other possible scenario is that an increase in evaporation may diminish the observed magnitude in SST rise.

5.3 Reconstructed Sr/Ca-SST and δ^{18}O-SSS: Pre-existing data series

ENSO, El Niño Southern Oscillation, is a source of interannual variability in the hydrological conditions of the tropical Pacific, with the signal appearing stronger in some years than others. National meteorological agencies, such as the National Oceanographic and Atmospheric Administration, use specific criteria to determine the occurrence and magnitude of an ENSO event. Two common methodologies are the Oceanic Niño Index (ONI) and the Southern Oscillation Index (SOI). The ONI, an average of SST over a region [5°N to 5° S, 170-120°W] called Niño 3.4, identifies an ENSO event when a 3-month running mean of SST anomalies exceeds ± .5°C for five consecutive months (NOAA, 2015). Measurements from the Niño 3.4 region recognize the ENSO events which cause notable SST anomalies in both the Niño 3 and 4 regions, with positive anomalies indicative of an ENSO warm phase event (figure 8). Although SOI has a similar signal magnitude and frequency as ONI, SOI indicates a warm phase event with a negative anomaly. SOI is the difference in standardized mean-sea level pressure between Darwin, Australia and Tahiti divided by the combined standard deviation. [Equation]

$$\text{SOI} = \frac{\text{(Standardized Tahiti - Standardized Darwin)}}{(\sum \text{(Standardized Tahiti - Standardized Darwin)}^2 / N)^{1/2}}$$

Indices used by national agencies often employ a threshold to identify an ENSO event. These thresholds only recognize ENSO once the ENSO signal reaches a certain strength, but ignore the connection between the interannual variability of hydrological conditions and ENSO. Several ENSO events of similar phase may occur in consecutive years, but are part of the same anomaly episode deviating from normal conditions. In order to investigate the natural frequency of ENSO's signal, this study adopted a threshold of zero to examine the interannual frequency of the detrended, reconstructed δ^{18}O-SSS and Sr/Ca-SST annual anomalies. Although this threshold does not identify the magnitude of an ENSO event, it does acknowledges the potential for an ENSO event.

Working with zero as the threshold, several calculations were produced using a moving 30-year period. For each unique centered 30-year period, the following measures were calculated:

1. The number of occurrences in which the data series fell above or below zero for a consecutive amount of time.
2. The average length of consecutive time in which a data series were above or below zero.

Calculation (1) shows the change in frequency of the interannual signal, which is related to ENSO, and calculation (2) shows the change in periodicity. For example, Figure ___ shows for the results of these calculations for New Caledonia Sr/Ca-SST. For the above threshold scenario in 1885 CE, the value 6 corresponds to calculation 1 and signifies that from 1870 to 1900 (i.e. the centered 30-year period around 1885), New Caledonia's detrended Sr/Ca-SST signal fell above zero six times. The value 3.33 for calculation (2) indicates New Caledonia's Sr/Ca-SST signal remained above the threshold on average for 3.33 years for any consecutive period of time from 1870 to 1900.

The detrended, reconstructed Sr/Ca-SST and δ^{18}O-SSS annual anomalies were unstandardized for these calculations. Alternatively, the individual values of these data series could have been standardized with a centered 30-year average and standard deviation. Standardization was not used because standardization did not significantly change the outcome of calculations; the correlation between the two methods was always above 0.9. The unstandardized data series were selected for examination because of their longer time series.

FIGURE 9, 10, 11 presents the results of individual sites for calculation (1) and (2), with solid lines representing above threshold scenarios and dashed lines representing below threshold scenarios. The linear trend of each scenario is also shown. There is a general negative correlation between calculation (1) and (2); an increase in the number of incidences above or below the threshold corresponds to a decrease in the

average length of those incidences for a unique 30-year period. However, there is more variation in the average interannual period than in the frequency number. A change in the results was deemed significant if the difference between two consecutive years was greater than one standard deviation, which was on average 1 for calculation (1) and .5 years for calculation (2). The outcome of calculations was different for each southwest Pacific site, but the trends and patterns for individual and between sites may be indicative of the SPCZ behavior over time.

Rarotonga data display the most change in the interannual signal over the course of its time series (1744 to 1976 CE) (figure 11). For both Sr/Ca-SST and δ^{18}O-SSS, the general linear trend shows an increase in frequency and decrease in period. More specifically though, the trend in frequency for reconstructed Sr/Ca-SST appears to display a shift in the average frequency at 1840 CE, increasing the average frequency from 5.8 to 7.5. The average periodicity for Sr/Ca-SST also appears to shift at 1840 CE. The shift is more significant for the above threshold scenario, in which the average period decreased from 2.9 years to 2.3 years. This trend is not as significant in the reconstructed δ^{18}O-SSS annual anomalies for Rarotonga, with an average of 5.5 from 1744-1840 CE and 6.9 from 1840-1976 CE for calculation (1). For calculation (2), the below threshold scenario experienced a larger shift, a decrease from 2.9 to 2.2 years, than the above threshold scenario.

The calculations for the New Caledonia data series (1667/1676 to 1972 CE) reveal a much different variability pattern than Rarotonga (figure 9). While there may be a slight shift in the Sr/Ca-SST frequency at 1740, the Sr/Ca-SST frequency remained fairly consistent from 1667 to about 1940, with the frequency centered on 6. There is a noticeable increase in the Sr/Ca-SST frequency during most of the 20th century. For the Sr/Ca-SST periodicity, the period for the above threshold scenario remained relatively constant while the below threshold scenario displayed a notable decreasing trend. The trend seen in δ^{18}O-SSS is quite different. Although the above and below threshold scenarios behave similarly for both calculations (1) and (2), there is a narrowing in the frequency and period ranges at around 1770 CE. The frequency range shrinks from a range of 9-4 for 1676-1770 CE to a range of 6-9 from 1770-1972 CE and the period range decreases from 3.75-1.5 years for 1676-1770 CE to a range of 2.83-1.4 years for 1770-1972 years.

Fiji data series show the least change in the variance of the interannual frequency, but also the largest, and most consistent range in frequency (figure 10). Although the average frequency remains constant for Sr/Ca-SST, there is a slight increase in range from 5-8 to a range of 4-8 at 1920 CE, with a greater occurrence of 8 as a frequency from 1960 to 1976. The period shows an increase in the average period for the below threshold scenario and slight increase in the range of periodicity for both scenarios. Changes in the δ^{18}O-SSS are more subtle, with a small shift in the range of frequency and periodicity at 1920, changing from 9-4 range to 10-6 range and from 4-1.3 years to 2.6-1.4 years, respectively.

5.4 *Reconstructed* Sr/Ca and $\delta^{18}O$: Aitutaki and Pre-existing data

The reconstructed Aitutaki data were examined in context with the pre-existing data and SOI. FIGURE 12 and 13 show the detrended, reconstructed Sr/Ca-SST and δ^{18}O-SSS annual anomalies standardized over two time periods, 1885-1920 CE and 1952-1987 CE (black line = New Caledonia, green line = Fiji, red line = Rarotonga, and blue line = Aitutaki). The black dashed line is the annually averaged SOI and the multi-colored dots are indicative of ENSO events of varying strength as determined by different thresholds using ONI.

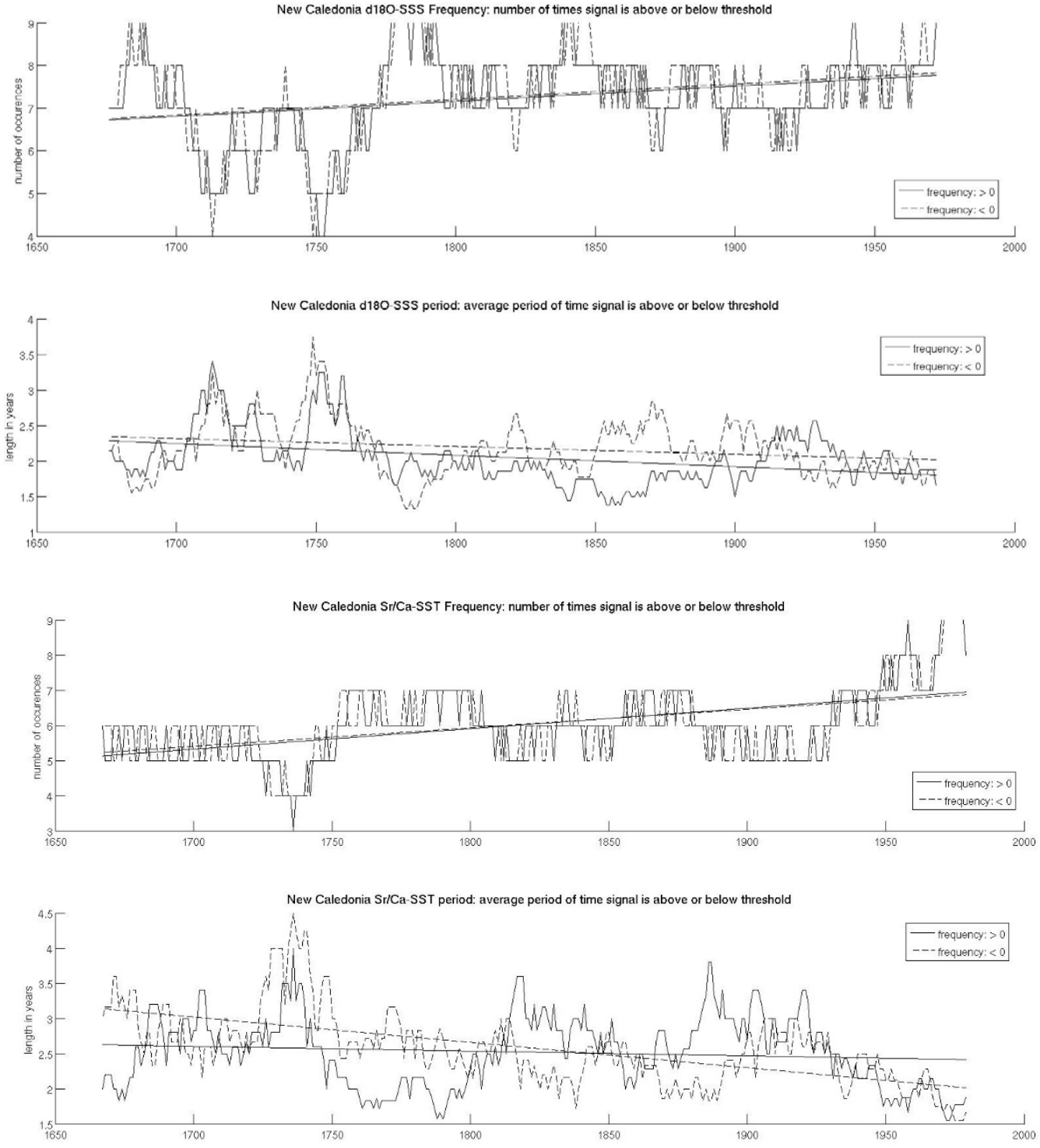

Figure 9: The change in the frequency and period for New Caledonia of a moving centered 30 year period for the occurrences above (solid line) and below (dashed line) zero with their corresponding linear trends. The uncertainty within the frequency is ± 1 and within the period ± .5 years.

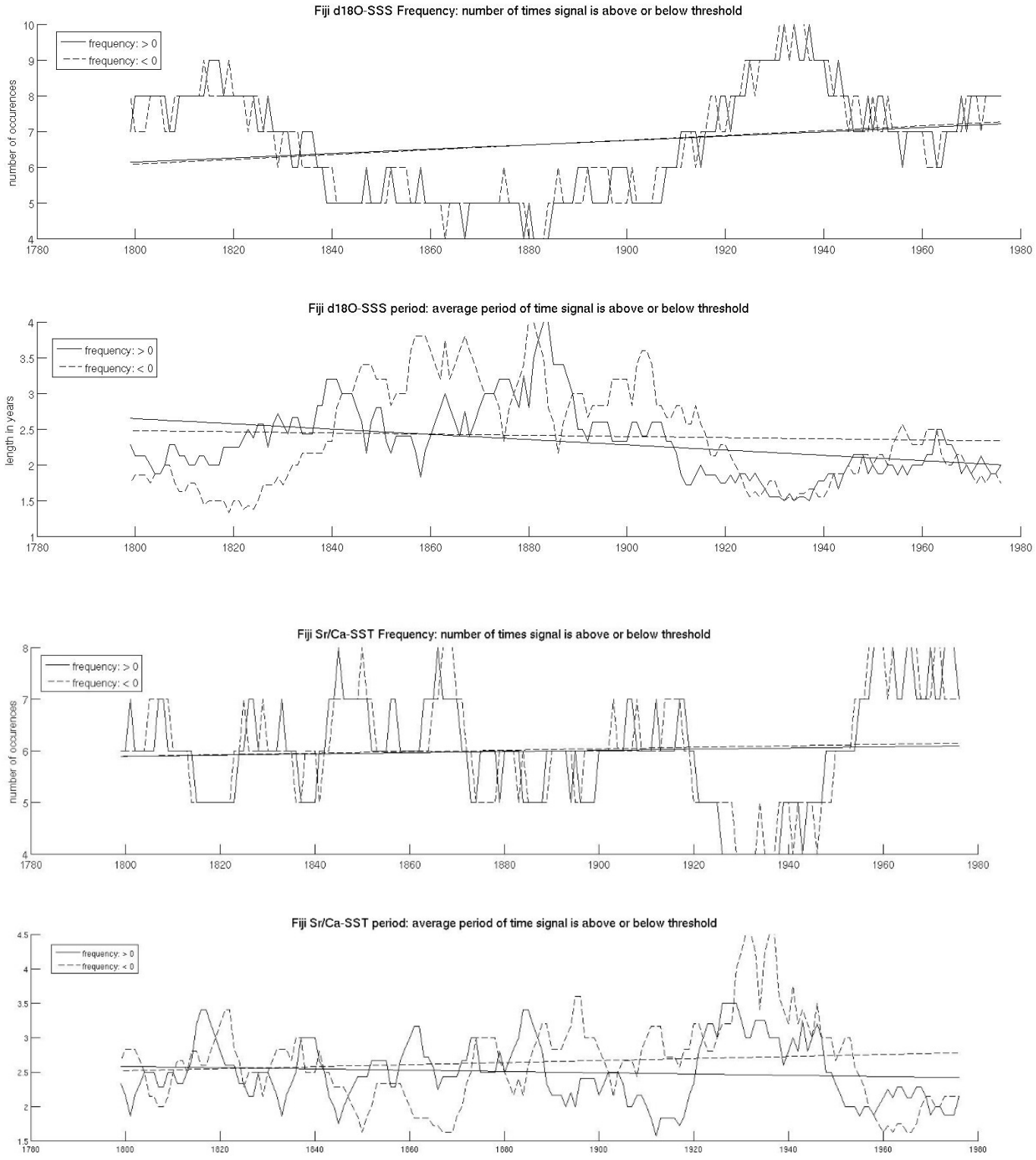

Figure 10: The change in the frequency and period for Fiji of a moving centered 30 year period for the occurrences above (solid line) and below (dashed line) zero with their corresponding linear trends. The uncertainty within the frequency is ± 1 and within the period ± .5 years.

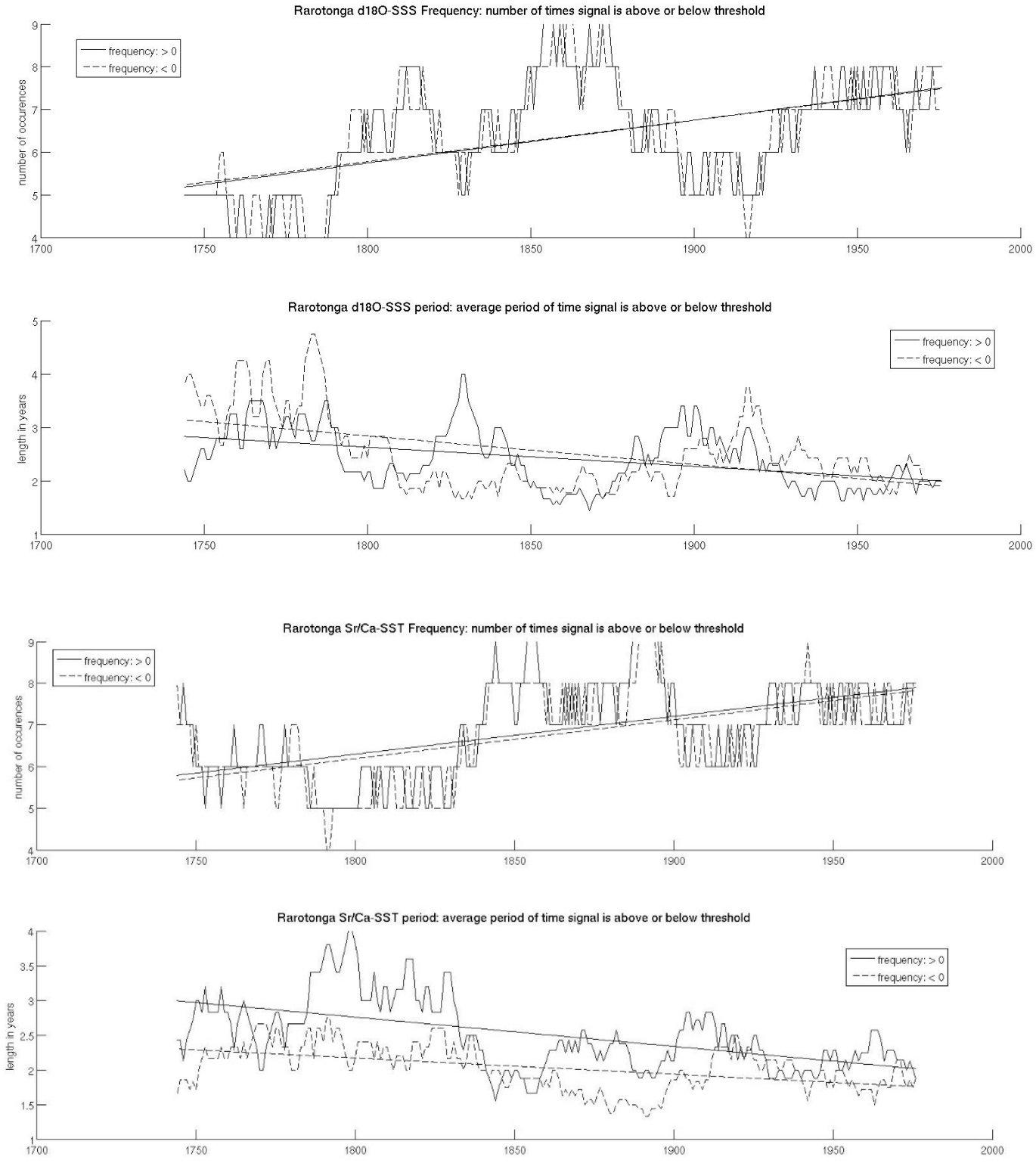

Figure 11: The change in the frequency and period for Rarotonga of a moving centered 30 year period for the occurrences above (solid line) and below (dashed line) zero with their corresponding linear trends. The uncertainty within the frequency is ± 1 and within the period ± .5 years.

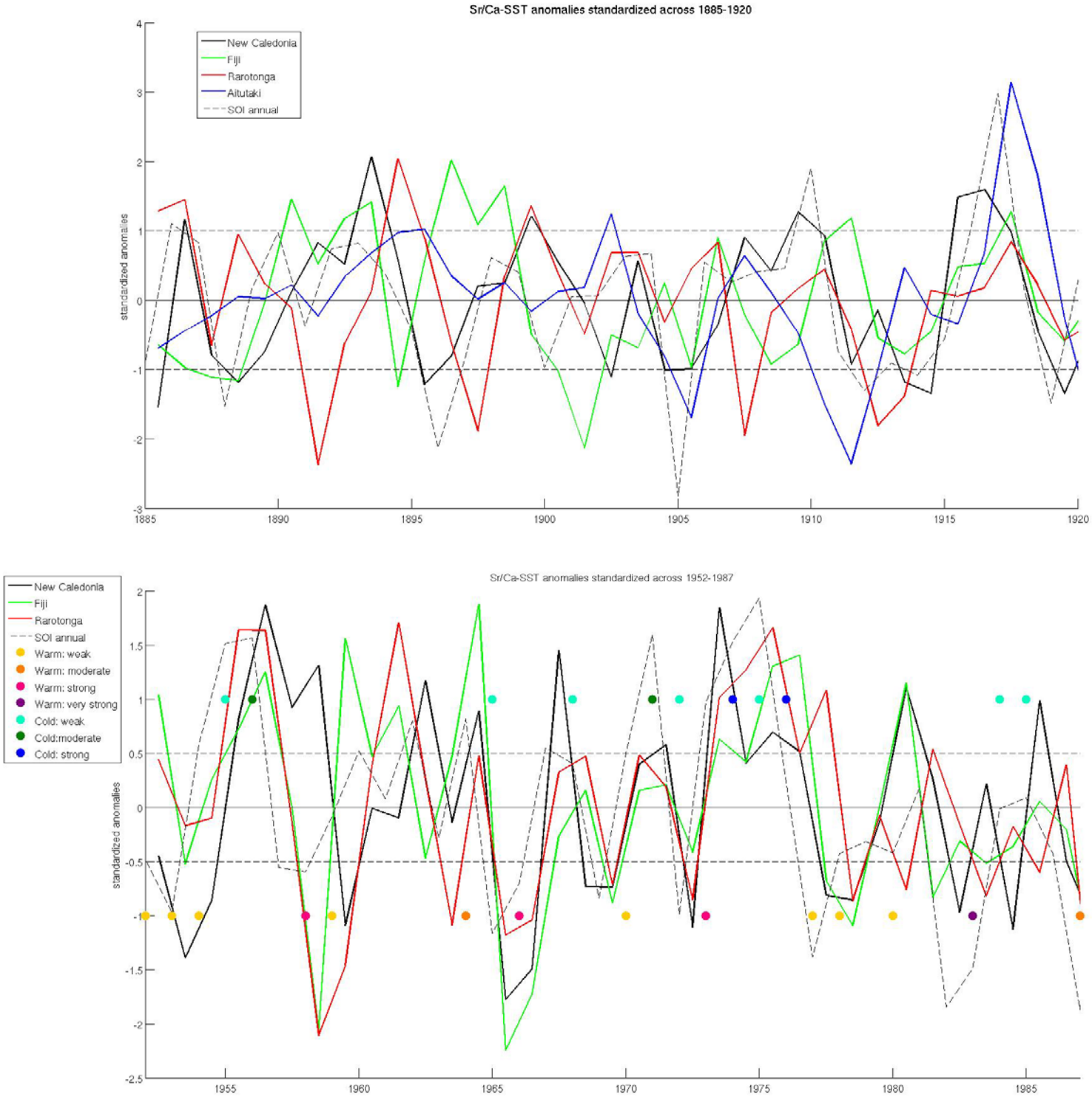

Figure 12: The detrended and standardized reconstructed Sr/Ca SST for 1885-1920 and 1952-1987 for New Caledonia (black), Rarotonga (red), Fiji (green), and Aitutaki (blue). The uncertainty within the all measurements is ± 27%. The multi-color dots correspond to ENSO phases of varying strength.

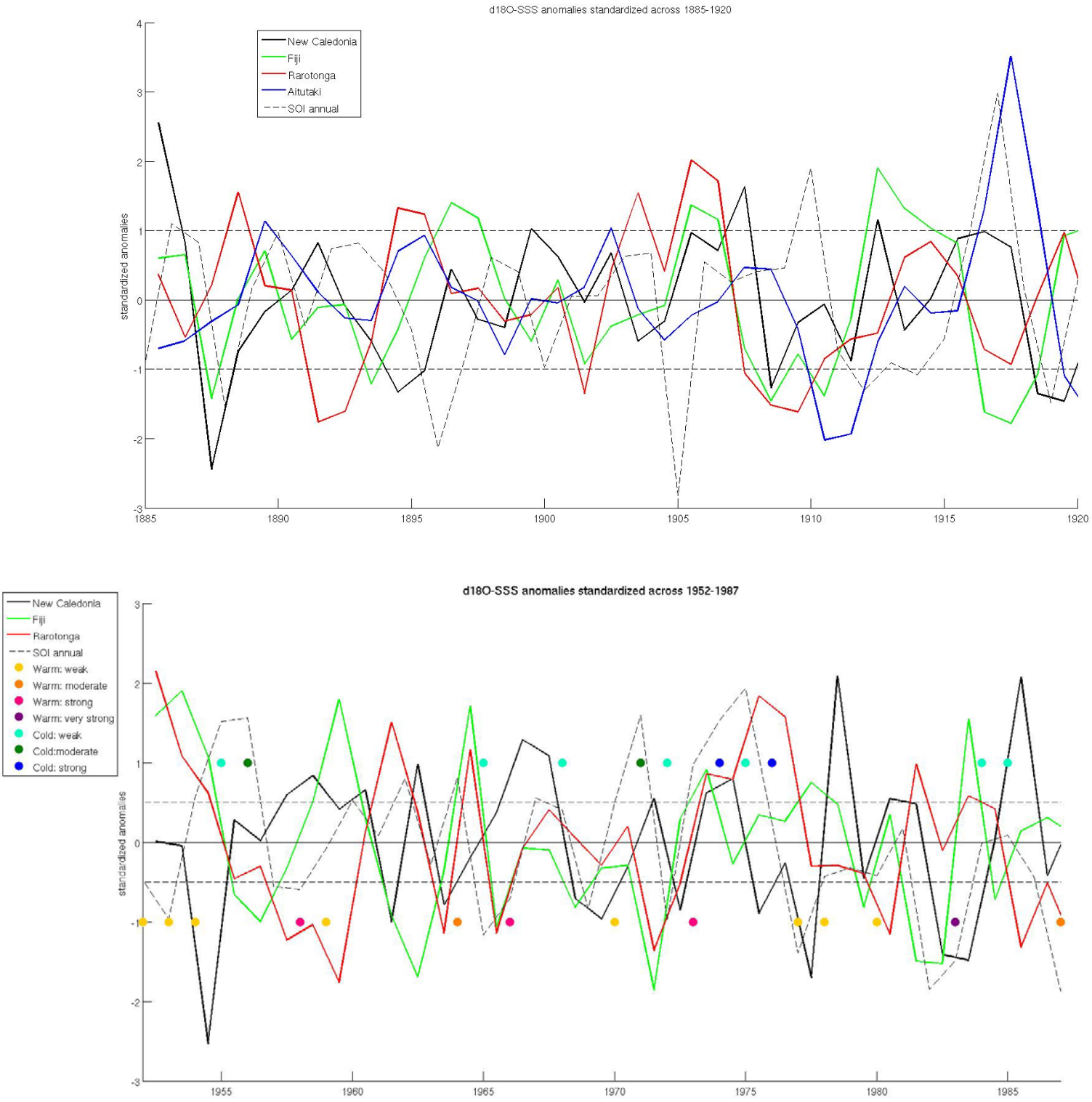

Figure 13: The detrended and standardized reconstructed d18O-SSS for 1885-1920 and 1952-1987 for New Caledonia (black), Rarotonga (red), Fiji (green), and Aitutaki (blue). The uncertainty within the all measurements is ± 27%. The multi-color dots correspond to ENSO phases of varying strength.

5.4.1 SOI vs. ONI

Figure 14 shows the 3-month running mean of ONI (gray line) and SOI (black line) (r = -.75, p = .17). To demonstrate the similarity between the two indices, SOI was inverted (dashed black line). The two indices differ in the month to month values but follow significantly similar annual trends, as shown in figure 15 (r = -.92, p = .72). Each multi-colored dot in figure 14 and 15 represents an ENSO event of varying strength, typically corresponding to a summer season spanning two years. For example, the magenta dot hovering between 1972 and 1973 indicates a strong warm ENSO phase that lasted from about July 1972 to March 1973. The strength of an ENSO event was determined by a series of ONI thresholds. Although the 3-month running mean ONI threshold for an ENSO event is ± .5°C, it was determined that a weak ENSO event lies between .5 to .9°C, a moderate event between 1 to 1.4°C, a strong event between 1.5 to 1.9°C, and a very strong event when ONI is greater than 2°C.

5.4.2 *Reconstructed* Sr/Ca-SST

The temperature signature of each southwest Pacific site is unique (figure 11). While correlation between sites was mostly significant, the detrended reconstructed Sr/Ca-SST annual anomalies are not identical. TABLE 3 and 4 displays the correlation coefficients and p-values of inter-site comparisons using unstandardized data from two time periods of interest. The correlation coefficient, r, remained the same for each inter-site comparison regardless of whether the data were standardized or not. While most correlations were positive, Fiji was negatively correlated to Rarotonga from 1885-1920 CE (r = -0.17). Excluding Aitutaki data, correlation between the remaining sites was higher for 1952-1987 CE (r = 0.4-0.56) than for 1885-1920 CE (r = -0.17- 0.20). The p-values remained well above the 0.05 significance level despite the time period. FIGURE 16 shows the 30-year moving correlation between New Caledonia and Rarotonga (black); New Caledonia and Fiji (green); and Fiji and Rarotonga (red). The value corresponding to a particular year is the correlation coefficient for a 30 year period centered on that year. Prior to 1910 CE, New Caledonia and Fiji individual correlations with Rarotonga fluctuated between positive and negative, and after, their correlation with Rarotonga became progressively more positive. The correlation between New Caledonia and Fiji is consistently positive but varies in strength throughout the decades. Correlations only began to coalesce around 1945 CE, when all inter-site correlations became increasingly positive. This coordinated increase suggests that regional SST anomalies are becoming more homogenous.

Whenever another site was compared to Aitutaki, the p-value plummeted to well below the 0.05 significance level. The 0.05 significance level represents a 5% probability the result is random and if a p-value fails to exceed this threshold, then the null hypothesis that the two data series are the same is rejected. The correlation coefficients from inter-site comparisons with Aitutaki are not significantly different from other coefficients for 1885-1920 CE.

When New Caledonia, Rarotonga, and Fiji were compared to SOI, their p-values were well above the 0.05 significance level and their correlation coefficients were positive. Because of these significant correlation; the standardized, reconstructed Sr/Ca-SST annual anomalies from New Caledonia, Fiji, and Rarotonga were used to identify ENSO events. Typically, an ENSO event is a consecutive time period of the same ENSO phase above a certain magnitude, such as the 1973-1976 CE La Niña (cold phase event). A cold phase event was identified when all three sites experienced a localized maximum within one year of each other, with at least two peaks occurring in the same year or a peak intersecting a high plateau of another site. A plateau formed when a year was similar in value before or after a localized maximum or minimum. A warm phase event was identified similarly but involved a localized minimum in the Sr/Ca-SST.

During the late 20th century (1952-1987 CE), 8 warm and 8 cold phase events were identified using the above method verses the 9 warm and 6 cold phase events identified using ONI (table 5). In general, the data-based ENSO events fell within ± 1 year of the ENSO events determined by ONI. The two extra

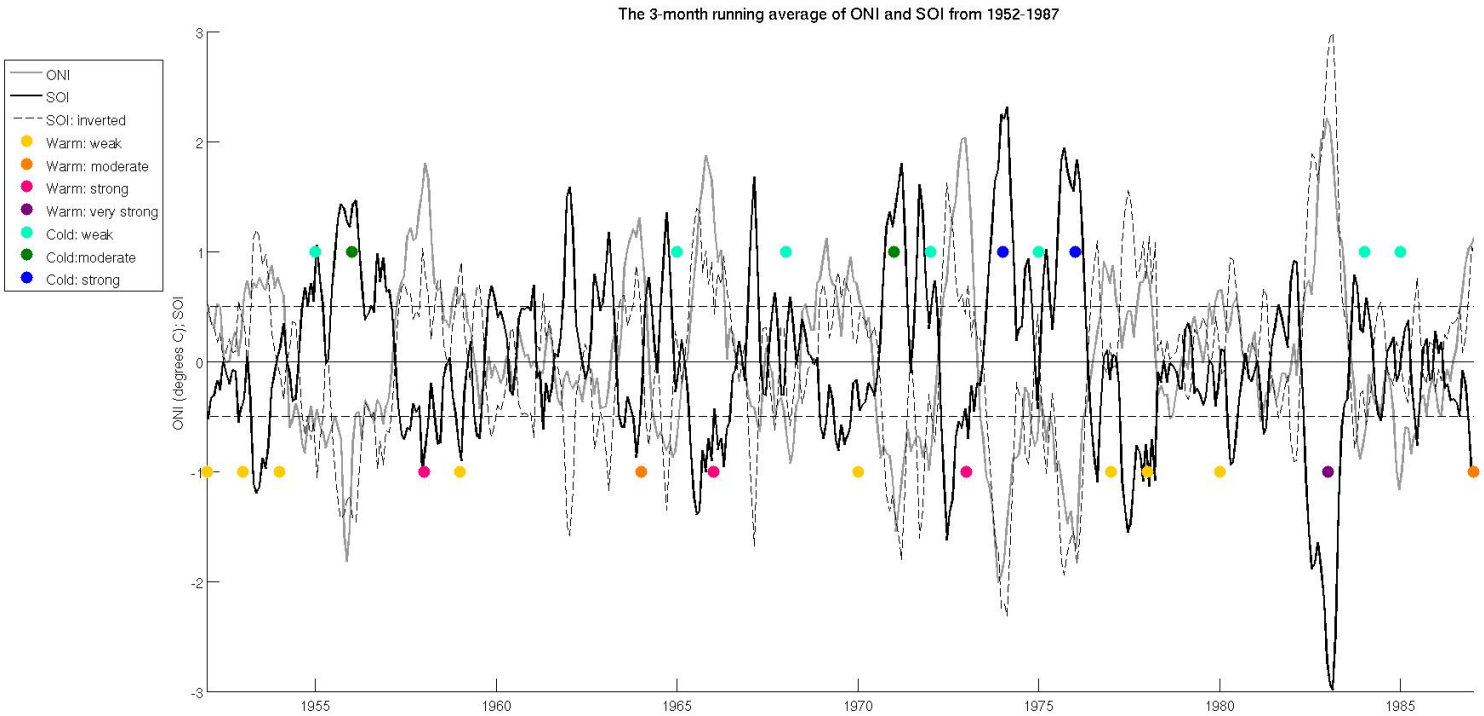

Figure 14: The 3 month running average for ONI (gray) and SOI (black). The inverted version of SOI is shown as the dashed black line. The multi-color dots correspond to ENSO phases of varying strength.

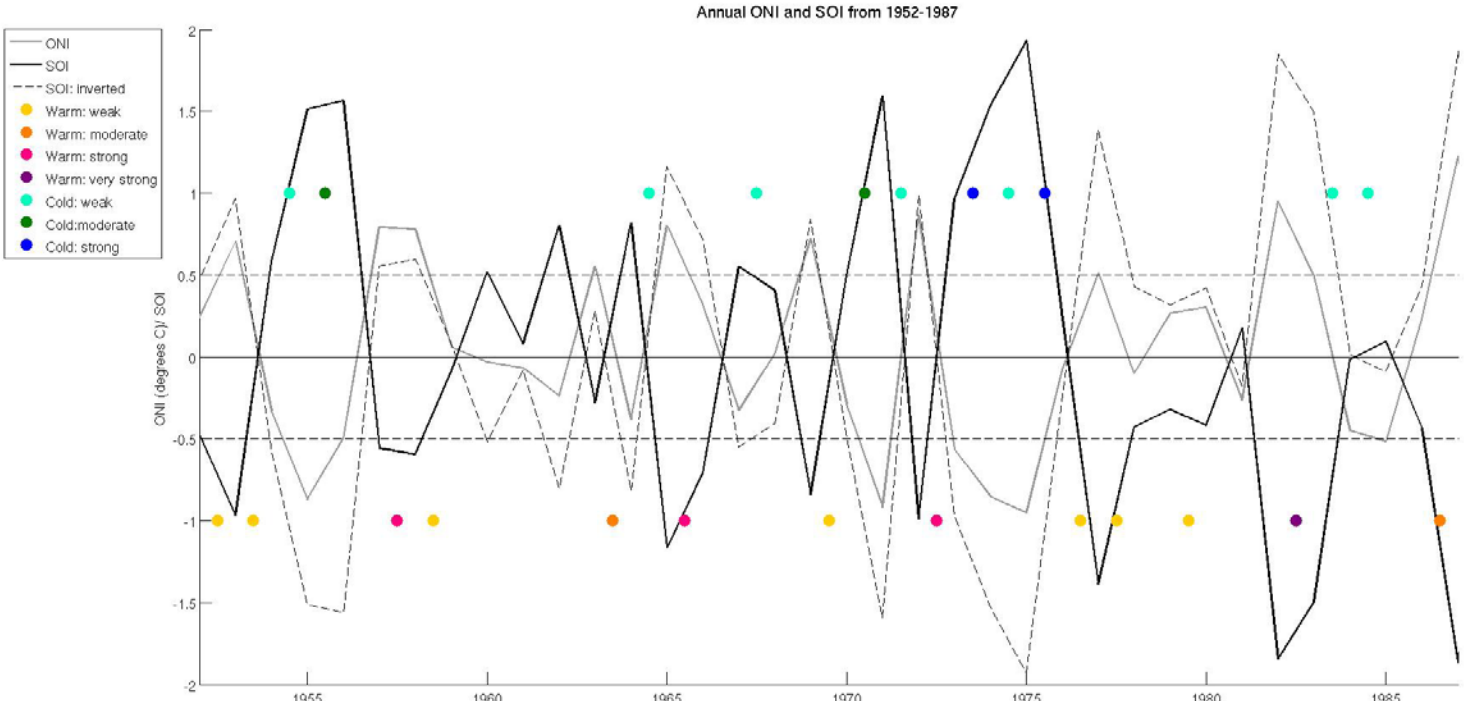

Figure 15: The annual average for ONI (gray) and SOI (black). The inverted version of SOI is shown as the dashed black line. The multi-color dots correspond to ENSO phases of varying strength.

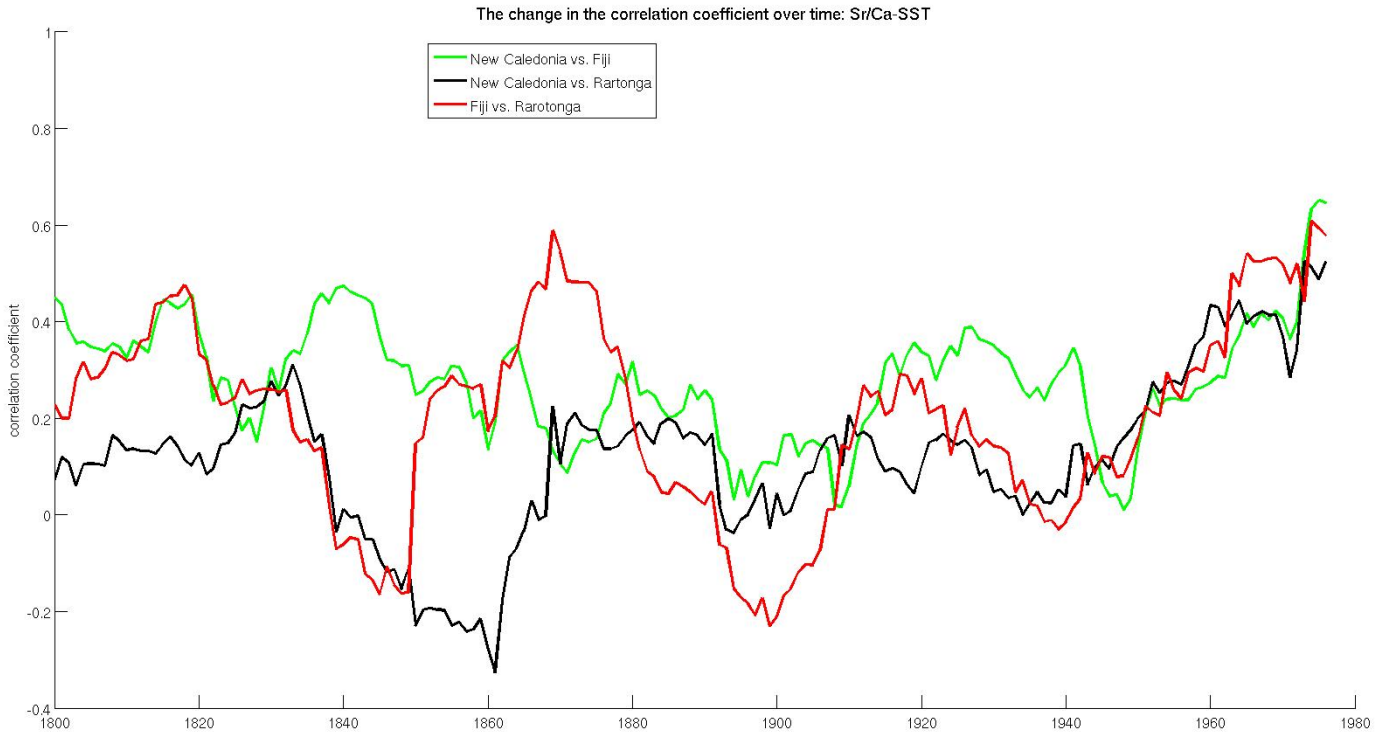

Figure 16: The change in the correlation coefficient over time for the Sr/Ca-SST of New Caledonia (black), Rarotonga (red), and Fiji (green).

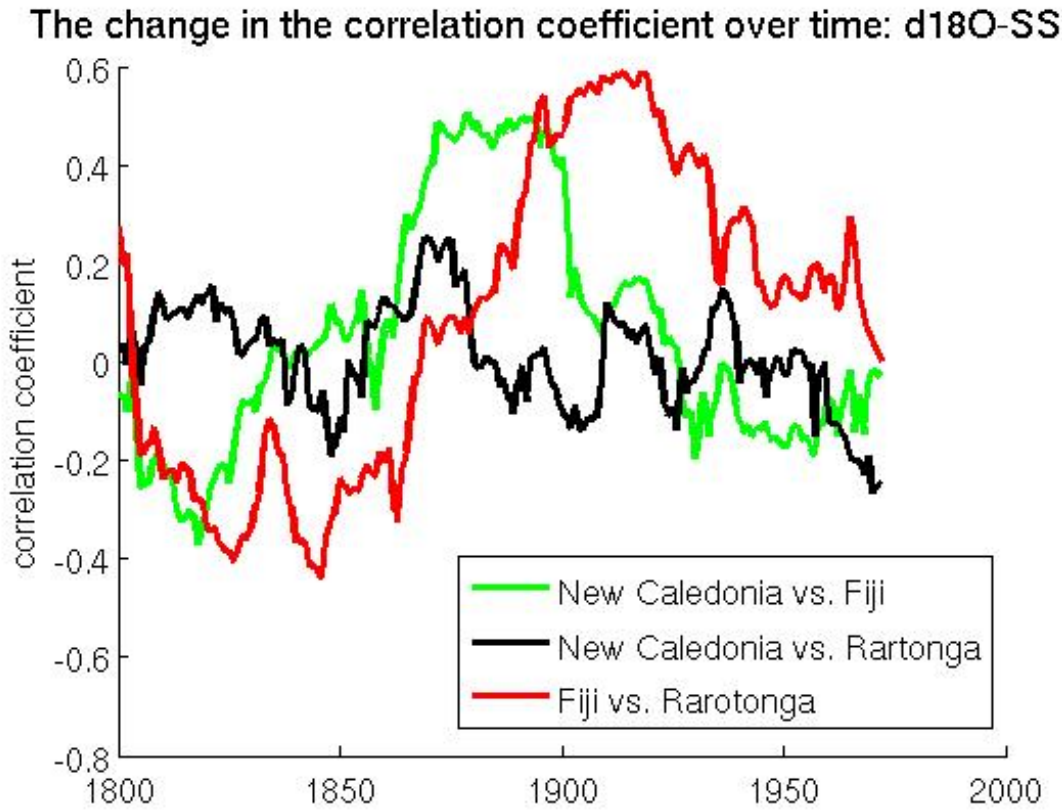

Figure 17: The change in the correlation coefficient over time for the d18O-SSS of New Caledonia (black), Rarotonga (red), and Fiji (green).

cold phase events, 1961 and 1980 CE, identified by data-based criteria were disregarded by the ONI criteria because the 3 month running ONI average did not exceed the ± 0.5°C threshold for five consecutive months. The data-based criteria missed a weak, warm event that occurred in 1979-80 CE, one year after another weak, warm event in 1976-1978 CE. During 1980 CE, the data-based criteria identified a cold-phase event instead of a warm-phase event because of the predominance of positive Sr/Ca-SST values.

From 1885-1920 CE, 5 warm phase and 6 cold phase events were identified using the data-based criteria whereas the SOI identified 6 warm and 7 cold phase events (table 6). SOI was used instead of ONI because the ONI data series does not extend past 1950 CE. Using SOI, an ENSO event was determined when the SOI 3-month running average exceeded ± 0.5 for five consecutive months. Once again, most data-based ENSO events fell within ± 1 year of the SOI determined years; however, there were some discrepancies. SOI identified cold phase events in 1887 and 1890 CE; during these years, the sign of Rarotonga and Fiji Sr/Ca-SST anomalies were opposite to that of Fiji. The data-based criteria also missed the 1896 CE warm event identified by SOI, because the local Sr/Ca-SST minimum of each site was too dispersed. Despite its poor correlation, most Aitutaki local minimums and maximums occured within ± 1 year of the data-based ENSO events.

Standardized, reconstructed Sr/Ca-SST annual anomalies were used to identify ENSO events rather than δ^{18}O-SSS because southwest Pacific sites share a similar SST anomaly pattern during ENSO events. The relationship between SST and ENSO is fairly simple; a negative SST anomaly corresponds to an ENSO warm phase event and a positive SST anomaly corresponds an ENSO cold phase event. The relationship between ENSO and SSS cannot be simplified as easily and must be examined on a site-to-site basis.

5.4.3 Reconstructed δ^{18}O-SSS

Most sites correlated positively with one another, expect for three occasions (table 9 and 10). Regardless of the time period, New Caledonia and Rarotonga were negatively correlated, as were Fiji and Aitutaki. The other negative correlation occurred between New Caledonia and Fiji during the late 20th century, but they correlated positively for 1885-1920 CE. From 1885-1920 CE, most δ^{18}O-SSS correlations were higher than Sr/Ca-SST correlations, but the opposite was true for 1952-1987 CE. Depending on which two sites were compared; some correlations rose with time, while others fell. When correlation coefficients were calculated over a 30-year moving period, there was significant variance between 30 year periods and between sites (figure 17). Correlation between New Caledonia and Rarotonga consistently fluctuated between positive and negative values, ranging from –0.2 to 0.2. Comparing New Caledonia and Rarotonga with Fiji produce correlation coefficients that range between -0.4 to nearly 0.6. These correlations with Fiji take a longer time to vary between positive and negative values than the correlation coefficients for the comparison between New Caledonia and Rarotonga.

Expect for comparisons with Aitutaki, the p-values of inter-site comparisons were significantly higher than the .05 significance level. The δ^{18}O-SSS p-values were higher than Sr/Ca-SST for 1885-1920 CE and 1952-1987 CE. Similar to Sr/Ca-SST comparisons made with Aitutaki, Aitutaki δ^{18}O-SSS data were insignificantly correlated to other southwest Pacific sites, with p-values well below the 0.05 significance level. Nevertheless when compared with SOI, Aitutaki had a p-value of 0.06. For the other sites, p-values for the SOI comparisons were very high, although slightly lower than the Sr/Ca-SST comparisons.

To investigate how SSS behaves for different southwest Pacific sites depending during each type of ENSO phase, the δ^{18}O-SSS anomaly and trend was examined from each ENSO event identified using Sr/Ca-SST (table 7). As with the change in correlation coefficients (figure 17), the relationships between sites are not consistent over time, nor is the behavior of an individual δ18O-SSS data series consistent with a phase of ENSO. Table 8 display the annual anomalies rounded to the nearest quarter (0.25 intervals) of δ^{18}O-SSS for 1885-1920 CE and 1952-1987 CE for both phases of ENSO. The blue or orange highlight signifies a negative or positive value, respectively. At first glance, it is difficult to discern a pattern in δ^{18}O-SSS values. The change from a positive to a negative anomaly for a particular site for a particular ENSO

phase may be related to a change in the magnitude of the ENSO phase. For example, Rarotonga values are generally positive for cold phase events and negative for warm-phase events. And yet, for the strong 1982-83 CE warm-phase event, Rarotonga experienced a positive SSS anomaly according to the data, a result possible if the SPCZ moved to far eastward. When looking at the magnitude and signs of various sites in comparison to one another and between ENSO phases, there is no apparent significant relationship. For the 1952-1987 CE period, the δ^{18}O-SSS trend was also analyzed by examining the change in annual anomalies from the year before to the year after an identified ENSO event. The trends of δ^{18}O-SSS did not elucidate any particular patterns either for an ENSO phase.

6. Discussion

6.1 Aitutaki

The poor correlation of Aitutaki data with other southwest Pacific sites and SOI may be attributed to the coral head selected to sample, how the coral sample was aged, and/or where Aitutaki is located in the southwest Pacific. When considering the core ATC13019B, the coral head is not the likely cause of the poor correlation. When choosing a coral head to sample, the head must be pristine and come from an environmental setting that reflects the hydrological variables being studied. The ATC13019B core was collected by Dr. Evans and PhD candidate Lopatka from a *Porites* coral head deposited on an eastern Aitutaki beach (Evans, 2011)). They speculated that a storm tore the coral head from nearby shallow water and deposited it on the beach. This is the most likely scenario, because the bulk and weight of a coral makes it difficult to transport, even under the force of a storm (Appendix for calculation of approximate force needed to move the coral head and further discussion). Also, *Porites* corals prefer to grow in shallow, warm waters, environmental conditions that match the shallow marine shelf fringing Aitutaki. As discussed in section *5.1.1* (Aitutaki Uncertainty), the results of diagenetic testing revealed ATC13019B to be 100% aragonite.

The age modeling of ATC13019B is also eliminated as a source of poor correlation, because the uncertainty associated with the age modeling is 0.12% of the data series total error (previously discussed in section *5.1.1*). Consequently, Aitutaki's location is the most likely cause for the poor correlation. Aitutaki lies at 18.85°S, 159.79°W, at the eastern edge of the SPCZ, the boundary between two opposing climate systems. The SPCZ's eastern edge is defined by the South Pacific Gyre, a counter-clockwise ocean circulation driven by the surface Trade Winds circling the South Pacific high pressure zone (Wildansky et al., 2010;). The sinking air in the South Pacific high pressure zone suppresses precipitation and the formation of clouds. In contrast, the low pressure trough that dictates the diagonal orientation of the SPCZ is a center for low-level convergence, an area where rising moist air condenses into clouds and precipitation (Vincent, 1993; Wildansky et al., 2010).

The climate signal recorded by Aitutaki coral may reflect a mixture of dry and saturated conditions as determined by the strength of the Trade Winds positioning the SPCZ. Table __ and __ display the rounded reconstructed δ^{18}O-SSS annual anomalies associated with ENSO events identified by the reconstructed Sr/Ca-SST anomalies for 1885-1920 CE. Regardless of the ENSO phase, Aitutaki δ^{18}O-SSS anomalies for a given ENSO event are typically lower than ± 0.25. The lack of divergence from the norm suggests that changes to the SPCZ induced by ENSO does not impact Aitutaki as significantly as other southwest Pacific sites. As shown in previous sections, the p-value analysis reveals that Aitutaki is statistically different from the other sites. With further analysis however, this difference may be used to advantage. Aitutaki sits on a climate node, which may or may not shift depending on the phase and strength of ENSO. When studying ENSO in the southwest Pacific, it is crucial to interpret the spatial variations in SSS to determine the position of the SPCZ. Aitutaki serves as a unique point of reference for comparisons to determine the ENSO phase and strength, and adds robustness to the analysis.

6.2 Hypothesis 1: Climatological averages and anomalies of SSS and SST from the Southwest Pacific have no statistical difference between the late 19th century and the 20th century.

The change in the southwest Pacific's climatology is subtle. Neither the Sr/Ca and $\delta^{18}O$ averages nor the average reconstructed $\delta^{18}O$-SSS and Sr/Ca-SST anomalies for individual sites were not statistically different between 1885-1920 CE and 1952-1987 CE. The Sr/Ca and $\delta^{18}O$ averages for the two time periods remained within 2 standard deviations of each other. The slight decrease in values may indicate warming SST in the tropical Pacific. The Tropics in general have a small annual range in SST, but the IPCC's Fifth Assessment Report noted an increase in surface temperatures of .4-.8°C from 1901-2012 CE (Stocker et al., 2013). When examining the changes in the average reconstructed $\delta^{18}O$-SSS anomalies, New Caledonia and Fiji data show a decrease in the average positive and negative anomaly, suggesting more wet conditions over time. Rarotonga anomalies shift towards more positive, indicating that 1952-1987 was drier than 1885-1920.

6.3 Hypothesis 2: There is no significant difference in the frequency of ENSO warm phases and cold phases between late 19th century and the late 20th century.

All the southwest Pacific sites, considered in this paper, lie within a narrow range of latitudes (-16° to -23°N) with New Caledonia located furthest west at 166.5°E, Rarotonga and Aitutaki located furthest east at -159.8°E, and Fiji positioned in between at 179.2°E. The SPCZ cuts diagonally across the meridional distribution of sites, with Fiji in the position most susceptible to the SPCZ's influence. When considering the change in the interannual signal's frequency and period (as discussed in section 5.3), Fiji reconstructed anomalies have the largest frequency range but the least variance in range over time. The frequency of Fiji reconstructed anomalies takes the longest time to vary from its highest value to its lowest. This behavior may indicate that the SPCZ interaction with ENSO, which is responsible for the interannual variance in the region, has a predictable pattern.

Similarly, the frequency for Rarotonga $\delta^{18}O$-SSS anomalies seems to also range widely during the entire time series (1744-1976 CE), but only from 1676-1770 CE for New Caledonia. If a large range in $\delta^{18}O$-SSS anomalies indicates the SPCZ's presence, then these results may imply that the SPCZ has shifted eastward. The narrow range in New Caledonia SSS anomalies suggests a decrease in the influence of SPCZ's interannual variance over the island's local area.

Although there is little change in the frequency of Fiji Sr/Ca-SST, there appears to be a shift in the average interannual frequency for Rarotonga and New Caledonia. Both data series show an increase in the frequency, which may correspond to a decrease in the range of SST. A decrease SST range would correlate well with an increase in global temperatures and a decrease in the zonal SST gradient. As mentioned in section 5.3, the average period for when Rarotonga Sr/Ca-SST anomalies fall above zero or when $\delta^{18}O$-SSS anomalies fall below zero shows a significant decrease. Sr/Ca-SST anomalies above zero indicate warmer than average conditions and $\delta^{18}O$-SSS anomalies below zero indicate conditions wetter than normal. A decrease in the period of the Sr/Ca-SST above threshold scenario and the $\delta^{18}O$-SSS below threshold scenario could indicate conditions, that were at one time anomalously warm or wet, are becoming the new norm. This scenario could indicate an increased presence of the SPCZ and warmer waters in the vicinity of Rarotonga.

The results presented here seem to agree with other studies that the SPCZ is expanding eastward (Linsley et al, 2006; Wu et al., 2013). Warmer global temperatures decrease the strength of the zonal temperature gradient in the Pacific, and weaken the mid-latitude circulation that controls the diagonal position of the SPCZ. With a weakened diagonal orientation, the SPCZ may reorient itself to become more aligned with the Equator. This shift in the SPCZ is similar to its behavior observed during an ENSO warm phase event. The frequency of ENSO events does not appear to have changed significantly from its natural variability as observed in the interannual signal for Fiji $\delta^{18}O$-SST annual anomalies. During the warming of the past 100 to 150 years, the potential for either ENSO phase has become more equal.

6.4 Future Work

This research addresses the frequency of ENSO phase events, but not the magnitude or intensity. Future work should concentrate on the inter-relations between the SSS anomalies of the southwest Pacific sites to

track the orientation of the SPCZ. The position of the SPCZ infers the phase of ENSO, and how far the position has shifted may be used to determine the intensity of ENSO. Observations should be compared to model simulations because if the model output is significantly similar to observations, the model will provide a better spatial resolution for analyzing the distribution SSS anomalies in the southwest Pacific. Models bring addition climatic variables to an analysis. Examining pressure and wind anomalies of the region may better explain observations and the variability of the SPCZ during ENSO phases. Most importantly, further sampling of the southwest Pacific should be pursued as more observations provide a stronger foundation for analysis and the validation of models. The Aitutaki data presented in this paper only spans 36 years, too short a time period to fully make use of its location on the node between the SPCZ and the South Pacific high pressure zone.

7. Conclusion

The scarcity of oceanic observations limits the scientific understanding of ENSO's natural variability. ENSO is a source of prominent interannual variability and it is unknown how its behavior may change with increasing global temperatures (Stocker et al., 2013). This research studied the interannual variability in reconstructed SST and SSS anomalies based on detrended Sr/Ca and $\delta^{18}O$ anomalies inputted into equation from Ren et al. (2002). New data from Aitutaki was examined along with pre-existing data from Rarotonga, Fiji, and New Caledonia. The Aitutaki data was found to be statistically different from the other sites, with p-values below the 0.05 significance level. The interannual frequency and period of New Caledonia, Fiji, and Rarotonga was chosen to be investigated in depth because those sites significantly correlated with SOI, an index used to ENSO phase events. Over a moving centered 30-year period, the measurements calculated were the number occurrences in which a data series fell above or below zero and the average period of those occurrences. The analysis found that the natural interannual frequency of the SPCZ, which is significantly correlated to ENSO, has not varied significantly over time, ranging between 4-9 occurrences of below/above zero periods in a 30-year period. The average Sr/Ca, $\delta^{18}O$, Sr/Ca-SST, and $\delta^{18}O$-SSS had not changed significantly between the late 19th century and the late 20th century. Based on the interannual analysis, there is evidence that suggests the SPCZ has expanded eastward, agreeing with previous studies (Linsley et al, 2006; Wu et al., 2013). Based on the frequency of times that fell above or below zero, the analysis determined the potential for either ENSO phase has become more equal over time. Although this study examined the natural frequency of ENSO, further research is needed to investigate the inter-site relationships in SSS anomalies across the southwest Pacific to better understand variations in ENSO's intensity.

8. Acknowledgements

I would like to thank the mentorship and advice of Dr. Michael Evans, Dr. Andrew Lorrey, and Ph.D candidate Alex Lopatka, and Rebecca Plummer for her guidance and help in the Paleoclimate Lab at the University of Maryland.

9. References

Alibert, Chantal, and Leslie Kinsley (2008), A 170-year Sr/Ca and Ba/Ca coral record from the western Pacific warm pool: 1. What can we learn from an unusual coral record?, *Journal of Geophysical Research*, vol. 113, C04008, doi:10.1029/2006JC003979.

Allison, N., A. A. Finch, S/ R/ Sutton, and M. Newville (2001), Strontium heterogeneity and speciation in coral aragonite: Implications for the strontium paleothermometer, *Geochimica et Cosmochimica Acta*, vol. 65, pp. 2699-2676.

Allison, Nicola, Adrian A. Finch, Jody M. Webster, and David A. Clague (2007), Palaeoenvironmental records from fossil corals: The effects of submarine diagenesis on temperature and climate estimates, *Geochimica et Cosmochimica Acta*, vol 71, pp. 4693–4703 doi:10.1016/j.gca.2007.07.02.

Allison, N., Itay Cohen, Adrian A. Finch, Jonathan Erez, Alexander W. Tudhope, and Edinburgh Ion Microprobe Facility (2014), Corals concentrate dissolved inorganic carbon to facilitate calcification, *Nature Communication*, vol. 5, doi:10.1038/ncomms6741.

Braconnot, Pascale, Sandy P. Harrison, Masa Kageyama, Patrick J. Bartlein, Valerie Masson-Delmotte, Ayako Abe-Ouchi, Bette Otto-Bliesner and Yan Zhao (2012), Evaluation of climate models using palaeoclimatic data, *Nature Climate Change*, Published online, DOI: 10.1038/NCLIMATE1456.

Carton, James A., and Benjamin S. Giese (2008), A reanalysis of Ocean Climate Using Simple Ocean Data Assimilation (SODA), *Monthly Weather Review*, vol. 136, pp. 2999-3017, DOI: 10.1175/200MWR1978.1.

Carilli, J. E., H. V. McGregor, J. J. Gaudry, S. D. Donner, M. K. Gagan, S. Stevenson, H. Wong, and D. Fink (2014), Equatorial Pacific coral geochemical records show recent weakening of the Walker Circulation, *Paleoceanography*, vol. 29, pp. 1031–1045, doi:10.1002/ 2014PA002683.

Corrège, Thierry (2006), Sea surface temperature and salinity reconstruction from coral geochemical tracers, *Paleogeography, Paleoclimatology, Paleoecology*, vol. 232, pp. 408-428, doi:10.1016/j.palaeo.2005.10.014

Cohen, Ann L., Grahma D. Layne, Stanley R. Hart, and Phillip S. Lobel (2001), Kinetic control of skeletal Sr/Ca in symbiotic coral: Implications for the paleotemperature proxy, *Paleoceanography*, vol. 16 (1), pp. 20-26.

DeLong, Kristine L., Terrence M. Quinn, and Frederick W. Taylor (2007), Reconstructing twentieth-century sea surface temperature variability in the southwest Pacific: a replication study using multiple coral Sr/Ca records from New Caledonia, *Paleoceanography*, vol. 22, PA4212, doi:10.1029/2007PA001444.

DeLong, Kristine L., Terrence M. Quinn, and Frederick W. Taylor, Ke Lin, and Chuan-Chou Shen (2012), Sea surface temperature variability in the southwest tropical Pacific since AD 1649, *Nature Climate Change*, vol. 2, pp. 799-804, DOI:10.1038/NCLIMATE1583.

De Villiers, Stephanie, Glen T. Shen, and Bruce K. Nelson (1994), The Sr/Ca temperature relationship in coralline aragonite: Influence of variability in $(Sr/Ca)_{seawater}$ and skeletal growth parameters, *Geochimica et Cosmochimica Acta*, vol. 58, pp. 197-208.

Done, Terry (2011), Corals: Environmental Controls on Growth, in *Encyclopedia of Modern Coral Reefs: Structure, Form and Process* (pp. 281-293), Springer.

Evans, Michael (2014), Project Description of P2C3: ENSO activity and the paleoclimatic context for interactions between climate, marine resources and human activity, National Science Foundation proposal.

Fairbanks, R. G, M. N. Evans, J. L. Rubenstone, R.A. Mortlock, K. Broad, M. D. Moore, and C.D Charles (1997), Evaluating climate indices and their geochemical proxies measured in corals, *Coral Reef*, vol. 16.

Frankowiak, Katarzyna, Maciej Mazur, Anne M. Gothmann, and JAROSŁAW Stolarski (2013), Diagenetic Alteration of Triassic Coral from Aragonite Konservat-Lagerstatte in Alakir Cay, Turkey: Implications for Geochemical Measurements, *PALAIOS*, vol. 28, pp. 333–342, DOI: 10.2110/palo.2012.p12-116r.

Gaetani, Glenn A., and Ann L. Cohen (2006), Element partitioning during precipitation of aragonite from seawater: A framework for understanding paleoproxies, *Geochimica et Cosmochimica Acta*, vol. 70, pp. 4617-4634.

Gagan, Michael K, Linda K. Ayliffe, David Hopley, Joseph A. Cali, Graham E. Mortimer, John Chappell, Malcolm T. McCulloch, and M. John Head (1998), Temperature and Surface-Ocean Water Balance of the Mid-Holocene Tropical Western Pacific, *Science*, vol. 279, pp. 1014-1018.

Gorman, M. K., T. M. Quinn, F. W. Taylor, J. W. Partin, G. Cabioch, J. A. Austin Jr., B. Pelletier, V. Ballu, C. Maes, and S. Saustrup (2012), A coral-based reconstruction of sea surface salinity at Sabine Bank, Vanuatu from 1842 to 2007 CE, *Paleoceanography*, vol. 27, PA3226, doi:10.1029/2012PA002302.

Hereid, Kelly A., Terrence M. Quinn, Frederick W. Taylor, Chauan-Cho Shen, R. Lawrence Edwards, and Hai Cheng (2012), Coral record of reduced El Niño activity in the early 15th to middle 17th centuries, *Geology*, published online, doi:10.1130/G33510.1.

Hirahara, Shoji, Masayoshi Ishii, Yoshikazu Fukuda (2014), Centennial-Scale Surface Temperature Analysis and Its Uncertainty, *Journal of Climate*, vol. 27, pp. 57-75.

Hopley, David (2011), Density and Porosity: Influence on Reef Accretion Rates, in *Encyclopedia of Modern Coral Reefs: Structure, Form and Process* (pp. 303-304), Springer.

Huang, Boyin, Viva D. Banzon, Eric Freedman, Lay Lawrimore, Wei Liu, Thomas C. Peterson, Thomas M. Smith, Peter W. Thorne, Scott D. Woodruff, and Huai-Min Zhang (2015), Extended Reconstructed Sea Surface Temperature Version 4 (ERSST.v4). Part 1: Upgrades and Intercomparisons, *Journal of Climate*, vol. 28, pp. 911-930, DOI: 10.1175/JCLI-14-00006.1.

Kiladis, George N., Hans von Storch, Harry van Loon (1989), Origin of the South Pacific Zone, *Journal of Climate*, vol. 2, pp. 1185-1195.

Kiladis, George N, and Kingtse C. Mo, (1998). Interannual and Interseasonal Variability in the Southern Hemisphere, In *Meteorology of the Southern Hemisphere* (pp. 307-336). American Meteorological Society.

Kinsman, David J.J, and H. D. Holland (1969), The co-precipitation of cations with $CaDO_3$—IV. The co-precipitation of Sr^{2+} with aragonite between 16° and 96°C, *Geochimica et Cosmochimica Acta*, vol. 22, pp. 1-17.

Linsley, B.K, G.M Wellington, D.P Schrag, L. Ren, M. J Salinger, and A.W Tudhope (2004), Geochemical evidence from corals for changes in the amplitude of South Pacific interdecadal climate variability over last 300 years, *Climate Dynamics*, vol. 22, pp. 1-11, DOI 10.1007/s00382-003-0364-y.

Linsley, B.K, Alexey Kaplan, Yeves Gourion, Jim Salinger, P. DeMenocal, Gerard Wellington, and Stephen Howe (2006), Tracking the extent of the South Pacific Convergence Zone since the early 1600s, *Geochemistry Geophysics Geosystems*, 7:4, doi:10.1029/2005GC001115.

Lough, J.M., and D.J. Barnes (2000), Environmental controls on growth of the massive coral Porites, *Journal of Experimental Marine Biology and Ecology*, vol. 245, pp. 225-243.

McGregor, H. V., and N. J. Abram (2008), Images of diagenetic textures in Porites corals from Papua New Guinea and Indonesia, *Geochem. Geophys. Geosyst.*, vol. 9, Q10013, doi:10.1029/2008GC002093.

McGregor, Helen V., and Michael K. Gagan (2003), Diagenesis and geochemistry of Porites corals from Papua New Guinea: Implications for paleoclimate reconstruction, *Geochimica et Cosmochimica Acta*, vol. 67, No. 12, pp. 2147–2156.

Meibom, A., S. Mostefaoui, J.-P. Cuif, Y. Dauphin, F. Houlbreque, R. Dunbar, and B. Constantz (2007), Biological forcing controls the chemistry of reef-building coral skeleton, *Geophys. Res. Lett.*, vol. 34, L02601, doi:10.1029/2006GL028657.

Meibom, A., M. Stage, J. Wooden, B. R. Constantz, R. B. Dunbar, A. Owen, N. Grumet, C. R. Bacon, and C. P. Chamberlain (2003), Monthly Strontium/Calcium oscillations in symbiotic coral aragonite: Biological effects limiting the precision of the paleotemperature proxy, *Geophys. Res. Lett.*, vol. 30 (7), 1418, doi:10.1029/2002GL016864.

NOAA (11/4/2015), Historical El Nino/La Nina episodes (1950-present), Retrieved 4/5/2015 from http://www.cpc.ncep.noaa.gov/products/analysis_monitoring/ensostuff/ensoyears.shtml.

Nothdurft, Luke D., and Gregory E. Webb (2009), Earliest diagenesis in scleractinian coral skeletons: implications for palaeoclimate-sensitive geochemical archives, Facies, vol. 55, pp. 161–201, DOI 10.1007/s10347-008-0167-z

Pichon, Michael (2011), Porites, In *Encyclopedia of Modern Coral Reefs: Structure, Form and Process* (pp. 815-821), Springer.

Quinn, T., and D. E. Sampson (2002), A multiproxy approach to reconstructing sea surface conditions using coral skeleton geochemistry, *Paleoceanography*, vol. 17 (4), pp. 1062, doi:10.1029/2000PA000528.

Quinn, T. M., F. W. Taylor, and T. J. Crowley (2006), Coral-based climate variability in the Western Pacific Warm Pool since 1867, *Journal of Geophysical Research*, vol. 111, C11006, doi:10.1029/2005JC003243.

Ren L., Braddock K. Linsley, Gerald M. Wellington, Daniel P. Schrag and Ove Hoegh-Guldberg (2002), Deconvolving the δ18O seawater component from subseasonal coral δ18O and Sr/Ca at Rarotonga in the Southwestern subtropical Pacific for the period 1726 to 1992, *Geochimica et Cosmochimica Acta*, vol. 67 (9), pp. 1609-1621.

Ruiz-Hernadez, Sergio, Ricardo Grau-Crespo, A. Rabdel Ruiz-Salvador, Nora H. De Leeuw (2010), Thermochemistry of strontium incorporation in aragonite from atomistic simulations, *Geochimica et Cosmochimica Acta*, vol. 74, pp. 1320-1328.

Schmidt, G.A., J.D Annan, P.J Bartlein, B.I. Cook, E. Guilyardi, J.C. Hargreaves, S.P. Harrison, M. Kageyama, A.N. LeGrande, B Konecky, S. Lovejoy, M.E Mann, V. Mason-Delmotte, C. Risi, D. Thompson, A. Timmermann, L.-B. Tremblay, and P. Yiou (2014), Using palaeo-climate comparisons to constrain future projections in CMIP5, *Climate of the Past*, vol. 10, pp. 221-250, doi:10.5194/cp-10-221-2014.

Schmidt, G.A., J. H. Jungclaus, C. M. Ammann, E. Bard, P. Braconnot, T. J. Crowley, G. Delaygue, F. Joos, N. A. Krivova, R. Muscheler, B. L. Otto-Bliesner, J. Pongratz, D. T. Shindell, S. K. Solanki, F. Steinhilber, and L. E. A. Vieira (2011), Climate forcing reconstruction for use in PMIP simulations of the last millennium (v1.0), *Geoscience Model Development*, vol. 4, pp. 33-45, doi:10.5194/gmd-4-33-2011.

Smith, S.V., R.W. Budemeier, R.C. Redalje, J.E. Houk (1979), Strontium-Calcium Therometry in Coral Skeletons, *Science*, vol. 204 (4391), pp. 404-407 doi: 10.1126/science.204.4391.404.

Stocker, T.F., D. Qin, G.-K. Plattner, L.V. Alexander, S.K. Allen, N.L. Bindoff, F.-M. Bréon, J.A. Church, U. Cubasch, S. Emori, P. Forster, P. Friedlingstein, N. Gillett, J.M. Gregory, D.L. Hartmann, E. Jansen, B. Kirtman, R. Knutti, K. Krishna Kumar, P. Lemke, J. Marotzke, V. Masson-Delmotte, G.A. Meehl, I.I. Mokhov, S. Piao, V. Ramaswamy, D. Randall, M. Rhein, M. Rojas, C. Sabine, D. Shindell, L.D. Talley, D.G. Vaughan and S.-P. Xie (2013), Technical Summary. In: Climate Change 2013: The Physical Science Basis. Contribution of Working Group I to the Fifth Assessment Report of the Intergovernmental Panel on Climate Change [Stocker, T.F., D. Qin, G.-K. Plattner, M. Tignor, S.K. Allen, J. Boschung, A. Nauels, Y. Xia, V. Bex and P.M. Midgley (eds.)]. Cambridge University Press, Cambridge, United Kingdom and New York, NY, USA.

Vincent, G Dayton (1993), The South Pacific Convergence Zone (SPCZ): a Review, *Monthly weather review*, vol. 122, pp. 1949-1970.

Vincent, D. G. (1998). Pacific ocean. In *Meteorology of the Southern Hemisphere* (pp. 101-117). American Meteorological Society.

Weber, Jon N. (1973), Incorporation of strontium into reef coral skeletal carbonate, *Geochimica et Cosmochimica Acta*, vol. 37, pp. 2173-2190.

Weber, Jon N. and Peter M. J. Woodhead (1972), Temperature Dependence of Oxygen-18 Concentration in Reef Coral Carbonates, Journal of Geophysical Research, vol. 77 (3).

Widlansky, Matthew J., Peter J. Webster, and Carlos D. Hoyos (2011), On the Location and orientation of the South Pacific Zone, *Clim Dyn*, vol. 36, pp. 561–578, doi: 10.1007/s00382-010-0871-6

Wu, H. C., B. K. Linsley, E. P. Dassié, B. Schiraldi Jr., and P. B. deMenocal (2013), Oceanographic variability in the South Pacific Convergence Zone region over the last 210years from multi-site coral Sr/Ca records, *Geochem. Geophys. Geosyst.*, vol. 14, pp. 1435–1453, doi:10.1029/2012GC004293.

Table 3: Reconstructed Sr/Ca-SST anomalies statistical comparisons amongst sites 1885-1920 CE (unstandardized)

Site	New Caledonia		Fiji		Rarotonga		Aitutaki	
	r	p	r	p	r	p	r	p
New Caledonia			0.19	0.70	0.03	0.65	0.19	0.02
Fiji	0.20	0.70			-0.17	0.88	0.12	0.02
Rarotonga	0.03	0.65	-0.17	0.88			0.17	0.03
Aitutaki	0.19	0.02	0.12	0.02	0.17	0.03		
SOI	0.56	0.95	0.23	0.93	0.24	0.87	0.38	0.03

Table 4: Reconstructed Sr/Ca-SST anomalies statistical comparisons amongst sites 1952-1987 CE (unstandardized)

Site	New Caledonia		Fiji		Rarotonga		Aitutaki	
	r	p	r	p	r	p	r	p
New Caledonia			0.42	0.86	0.40	0.90		
Fiji	0.42	0.86			0.56	0.78		
Rarotonga	0.40	0.90	0.56	0.78				
Aitutaki								
SOI	0.61	0.94	0.58	0.88	0.66	0.99		

Table 5: Reconstructed d18O-SSS anomalies for years identified as ENSO events by Sr/Ca-SST Cold phase (1952-1987)

Year	New Caledonia	Fiji	Rarotonga
1956	~ 0.0	(-) ~ 0.25	(-) ~ 1
1961	(-) ~ 1	(-) ~ 1	(+) ~ 1.5
1964	~ 0.0	(+) ~ 1.75	(+) ~ 1
1968	(-) ~ 0.75	(-) ~ 0.75	(+) ~ 0.0
1971	(+) ~ 0.5	(-) ~ 1.75	(-) ~ 1.25
1975	(-) ~ 0.75	(+) ~ 0.25	(+) ~ 1.75
1980	(+) ~ 0.5	(+) ~ 0.25	(-) ~ 1.25
1985	(+) ~ 2	(+) 0.25	(-) ~ 1.25

Table 6: Reconstructed d18O-SSS anomalies for years identified as ENSO events by Sr/Ca-SST Cold phase (1952-1987)

Year	New Caledonia	Fiji	Rarotonga
1956	~ 0.0	(-) ~ 0.25	(-) ~ 1
1961	(-) ~ 1	(-) ~ 1	(+) ~ 1.5
1964	~ 0.0	(+) ~ 1.75	(+) ~ 1
1968	(-) ~ 0.75	(-) ~ 0.75	(+) ~ 0.0
1971	(+) ~ 0.5	(-) ~ 1.75	(-) ~ 1.25
1975	(-) ~ 0.75	(+) ~ 0.25	(+) ~ 1.75
1980	(+) ~ 0.5	(+) ~ 0.25	(-) ~ 1.25
1985	(+) ~ 2	(+) 0.25	(-) ~ 1.25

Table 7: Reconstructed d18O-SSS anomalies for years identified as ENSO events by Sr/Ca-SST Warm phase (1885-1920)

Year	New Caledonia	Fiji	Rarotonga	Aitutaki
1888	(-) ~ 0.75	~ 0.0	(+) ~ 1.5	~ 0.0
1901	~ 0.0	(-) ~ 0.75	(-) ~ 1.25	(+) ~ 0.25
1904	(-) ~ 0.25	~ 0.0	(+) ~ 0.5	(-) ~ 0.5
1913	(-) ~ 0.25	(+) ~ 1.25	(+) ~ 0.75	(+) ~ 0.25
1919	(-) ~ 1.5	(+) ~ 1	(+) ~ 1	(-) ~ 1

Table 8: Reconstructed d18O-SSS anomalies for years identified as ENSO events by Sr/Ca-SST Cold phase (1885-1920)

Year	New Caledonia	Fiji	Rarotonga	Aitutaki
1893	(-) ~0.5	(-) ~ 1	(-) ~ 0.5	(-) ~ 0.25
1899	(+) ~ 1	(-) ~ 0.5	(-) ~ 0.25	~ 0.0
1903	(-) ~ 0.5	(-) ~ 0.25	(+) ~ 1.5	(-) ~ 0.0
1906	(+) ~ 0.75	(+) ~ 1.25	(+) ~ 1.75	~ 0.0
1910	0.0	(-) ~ 1.5	(-) ~ 0.75	(-) ~ 2
1917	(+) ~ 0.75	(-) ~ 1.75	(-) ~ 0.75	(+) ~ 3.5

Table 9: d18O-SSS anomalies statistical comparisons amongst sites 1885-1920 CE (standardized)

Site	New Caledonia		Fiji		Rarotonga		Aitutaki	
	r	p	r		r	p	r	p
New Caledonia			0.23	1.0	-0.13	1.0	0.10	1.0
Fiji	0.23	1.0			0.48	1.0	-0.32	1.0
Rarotonga	-0.13	1.0	0.48	1.0			0.0013	1.0
Aitutaki	0.10	1.0	-0.32	1.0	0.0013	1.0		

Table 10: Reconstructed d18O-SSS anomalies statistical comparisons amongst sites 1952-1987 CE (standardized)

Site	New Caledonia		Fiji		Rarotonga		Aitutaki	
	r	p	r	p	r	p	r	p
New Caledonia			-0.11	1.0	-0.27	1.0		
Fiji	-0.11	1.0			0.21	1.0		
Rarotonga	-.027	1.0	0.21	1.0				
Aitutaki								

10. Appendix

Table 1: Equations used to detrend annual Sr/Ca data series (y = Sr/Ca, x = year)	
Site	**Long-term trend equations**
New Caledonia	$y = -1E\text{-}06x^2 + 0.0048x + 4.8468$ and then, $y = -0.0011x + 1.0046$
Fiji	$y = -4E\text{-}06x^2 + 0.0134x - 3.1612$ and then, $y = 0.0014x - 1.3033$
Rarotonga	$y = -5E\text{-}06x^2 + 0.0174x - 7.2107$ and then, $y = 0.0017x - 1.5428$
Aitutaki	$y = -7E\text{-}05x^2 + 0.282x - 257.25$ and then, $y = -0.0179x + 16.979$

Table 2: Equations used to detrend annual d18O data series (y = d18O, x = year)	
Site	**Long-term trend equations**
New Caledonia	$y = -6E\text{-}06x^2 + 0.0211x - 22.683$ and then, $y = -6E\text{-}05x + 0.097$
Fiji	$y = -9E\text{-}06x^2 + 0.0301x - 31.434$ and then, $y = 0.0019x - 1.7552$
Rarotonga	$y = -2E\text{-}06x^2 + 0.0075x - 9.7151$ and then, $y = -0.0017x + 1.5997$
Aitutaki	$y = 0.0002x^2 - 0.5913x + 560.51$ and then, $y = -0.1724x + 163.98$

Calculation of force to move ATC13019B coral head

The cross-section of sample ATC13019B's coral head is approximately 36 ft^2 (calculated using the *Rite in the Rain* field book in FIGURE as reference) and a approximate bulk density of 1-2.2 g/cm^3 (Hopley, 2011). A 36 ft^2 x 1 ft cross-sectional volume is 3.34 x 10^6 cm^3 and when multiplied by 1 g/cm^3, the product is 3.34 x 10^6 g. This weight is equivalent to 3.68 tons, which would require about 3.6 x 10^7 N to move. The wind

Even though cyclone winds would be strong enough to move this weight, the bulk of the coral head would limit how far it is transported. The other factor to consider is the water depth of the coastal shelf next to the beach on which the coral head was found. The width of the shelf is about 1360 meters and slowly slopes downward up to a depth of about 40 meters before the seafloor drops 100 meters in the less than 400 meters (measured from Google earth). Because a *Porites'* growth is limited by the availability of sunlight, the coral head cannot have originated much farther past the shelf.